Dynamics of Mitotic Microtubules in Fission Yeast

by

Patrick John Flynn

Bachelor of Arts – Department of Physics

Undergraduate Honors Thesis

Final Copy

Thesis Defense Committee:

Meredith Betterton	Advisor	Department of Physics
Mike Ritzwoller	Honors Council Representative	Department of Physics
Richard J. McIntosh	External Faculty Member	Department of MCD Biology

Defended:

April 11^{th}, 2017

This thesis entitled:
Dynamics of Mitotic Microtubules in Fission Yeast
written by Patrick John Flynn
has been approved for the Department of Physics

_____

Dr. Meredith Betterton

_____

Dr. Michael Ritzwoller

_____

Dr. Richard McIntosh

Date _____

The final copy of this thesis has been examined by the signatories, and we find that both the content and the form meet acceptable presentation standards of scholarly work in the above mentioned discipline.

Flynn, Patrick John (B.A., Physics)

Dynamics of Mitotic Microtubules in Fission Yeast

Thesis directed by Dr. Meredith Betterton

Abstract

Microtubules (MTs) are cytoskeletal polymers that assemble into a biomechanical complex known as the mitotic spindle. The spindle is responsible for the equal partitioning of chromosomes during cell division; an event known as mitosis. The dependence of proper chromosome segregation on the dynamics of individual microtubules (MTs) is not well understood or easy to study due to their small size and quick dynamics. Mathematical models and simulations have been constructed in order to better understand the physical basis of how the mitotic spindle accurately, or inaccurately, divides duplicated chromosomes during mitosis. These models rely on the dynamics parameters of individual MTs, some of which are difficult to measure due to the resolution limits of live cell microscopy. This research has better quantified the dynamics of mitotic MTs in an effort to further restrict parameter ranges implemented in simulations of mitosis. Using biological and computational methods, I created a microscopy protocol to image fission yeast cells stalled in early mitosis and developed a pipeline that allows for the direct analysis of MT dynamics from raw micrograph data. I also conducted various bleaching experiments to determine kinetics of unresolvable MTs during spindle formation. I developed a kinetic Monte Carlo simulation of the stalled mitotic spindle that can be used to generate simulated data to benchmark the performance of the analysis techniques. This work has better defined parameter ranges for the dynamics of mitotic microtubules, values critical for accurate simulation of chromosome segregation, as well as developed a computational pipeline that may be applicable to a wide range of other biological microscopy data.

Dedication

I dedicate this to my Mother and Father.

"Fare you well, fare you well

I love you more than words can tell"

- Hunter & Garcia

Acknowledgements

Special thanks to Dr. Meredith Betterton, Dr. Dick McIntosh, and Zach Gergely who made this research possible. I would also like to thank the UROP at CU Boulder for providing funding for the beginning of this research project.

Contents

Chapter

Figures

Figure

Chapter 1

Mitosis, Microtubules and Fluorescence Microscopy

Cellular replication is essential for life. The long term viability of any species depends on the ability of individual organisms to survive and reproduce. Organismal reproduction begins on the cellular level and requires the proper coordination of many complex mechanochemical events in order to produce viable daughter cells. A large portion of the cell's life is spent in preparation for division. A diagram of the cell's life cycle (see figure 1.1) shows how prominent mitosis is because, although relatively short, the majority of the metabolic effort in each of the other phases are in preparation for cell division. G phases refer to the gap phases of the cell cycle when it is growing and producing proteins, but not replicating or dividing, and S phase refers to when the cell replicates its DNA. These non division phases of the cell cycle are often grouped together in the term interphase which implies that the cell is not currently dividing. Interphase ends with cell division in which one cell produces two daughter cells who now begin their own cell cycles. This repetitive cyclic pattern of life is common to most cells and is often perturbed in unhealthy cells [1, 2].

The biochemical pathways and physical mechanisms involved in the division of a cell into two daughter cells can be separated into two distinct phases, mitosis and cytokinesis. Mitosis refers to the division of genetic information, in the form of chromosomes, by the mitotic spindle into each of the new daughter cells. Cytokinesis describes the partition of the parent cell's continuous membrane into two separate membranes for each daughter cell. Mitosis can be thought of as a division in information and cytokinesis as a division in space. Another distinguishing characteristic

between these events is that the primary cytoskeletal polymer utilized in mitosis is microtubules, whereas cytokinesis primarily uses actin. Although there is active research into the underlying mechanisms that allow each phase of cell division to occur, and to do so in a tightly controlled and accurate manner, this thesis focuses on the process of mitosis in the context of the individual microtubule [MT] polymers that comprise the mitotic spindle and segregate chromosomes.

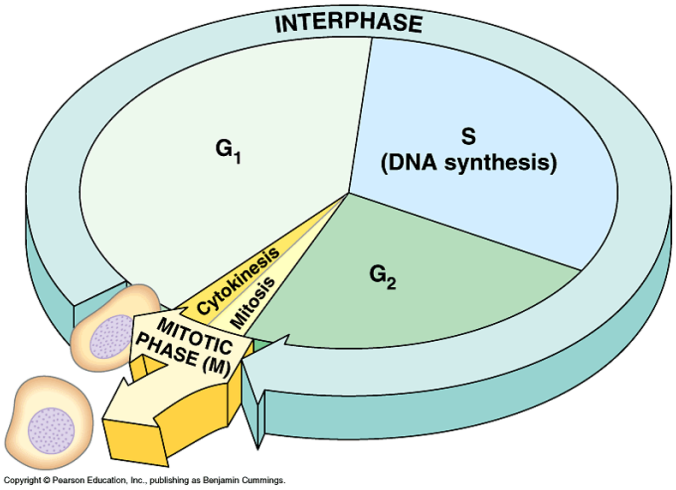

Figure 1.1: Example cycle that cells undergo. This thesis focuses on the phase of the cells life called mitosis, in which the replicated genetic information is separated by the mitotic spindle. (Image Credit: http://www.bio.utexas.edu/faculty/sjasper/bio212/mitosis.html)

1.1 Mitosis

Mitosis is the critical stage of the cell's life cycle in which it equally divides its replicated genetic material to pass on to the two new daughter cells. The term mitosis comes from the Greek word *mitos* meaning thread and was originally coined by Walter Flemming in the 1880s to describe the process of chromosome segregation, because of the similar looking structure between the mitotic spindle and a spool [2, 3]. The mitotic spindle is a self assembling multi-molecular structure containing microtubules (MTs) and proteins that accurately divide the chromosomes into separate ends of the dividing cell. The mitotic spindle is common to all eukaryotic cells and is an area of intense research because of its conserved mechanics and biological importance. [2, 3, 4] The

MTs are an important cytoskeletal polymer that serves many different roles in the cell and are a subject of studies themselves, as well as when a component in the spindle [5, 6, 7, 8, 9]. Recent technical progress in microscopy and genetic engineering are permitting researchers to study and perturb mitosis with imaging that allows for finer resolution of the molecular detail underlying the structure of the mitotic spindle and its proper functioning.[10, 11, 12]

Mitosis consists of four general stages: Prophase, Metaphase, Anaphase, and Telophase. The division of mitosis into these phases was first described by Mayzel in 1875 and visualized in a drawing by Flemming [2, 13]. Each of these phases is defined by differences in cellular organization and molecular activity. The defining characteristic of these four stages of mitosis is the state of the chromosome-spindle complex. Prophase in fission yeast is when the spindle pole bodies (SPBs) become embedded in the nuclear envelope and begin nucleating MTs that serve as the basis of the mitotic spindle. At the end of prophase, the chromosomes are fully condensed into sister chromatids and each connected to MTs nucleating from a SPB, and the mitotic spindle has preliminarily formed between the SPBs. During metaphase, the MTs align the chromosomes on the spindle in an organizational pattern known as the metaphase plate in which all of the chromosomes are aligned on a perpendicular plane to the spindle axis [2, 13]. A regulatory mechanism called the spindle assembly checkpoint (SAC) controls the anaphase wait signal that prevents premature spindle elongation and chromosome division by pausing until the proper formation of the spindle and alignment of the chromosomes on the metaphase plate [4, 14]. Clearance of the checkpoint depends on some combination of the connection of chromosomes with MTs and the tension balance resulting from the proper alignment of the chromosomes on the spindle which leads to the satisfaction of the checkpoint, allowing the cell to transition from metaphase into anaphase [13, 15]. Anaphase is marked by the elongation of the mitotic spindle and movement of the sister chromatids towards each pole body. After anaphase completes and the sister chromatids are partitioned into separate halves of the cell, telophase initiates. This phase is defined by the dissolution of the mitotic spindle and completion of chromosome segregation. The end of telophase marks the completion of mitosis; cytokinesis now begins with the cell physically dividing its membrane into two new daughter cells.

Early mitosis has been subdivided into more specific and distinguishable phases. A portion of my research has focused on the transition between prophase and metaphase, known as prometaphase. Prometaphase is the stage of mitosis in which the spindle is actively forming from its MT and protein components [2, 16]. Prometaphase is also the phase in which chromosomes become connected to MTs in order to prepare for the alignment on the metaphase plate. Spindle construction and chromosome capture are two essential mechanisms that must occur for proper chromosome segregation. There is a complicated, interconnected relationship between the individual MTs, the mitotic spindle, and the chromosomes during this phase of mitosis [2, 5, 9, 17]. The mitotic spindle system is a biological structure that performs a physical feat essential for life, yet remains incompletely understood.

Failure in spindle formation or chromosome attachment leads to the wrong number of chromosomes, which makes the cell genetically and metabolically unstable [18, 19, 20]. Aneuploidy describes cells that have an aberrant number of chromosomes and results from a cell undergoing an improper mitosis. Unequal chromosome segregation often leads to cell death, but also contributes to various illnesses, such as cancer or Down syndrome [3, 19]. The correct functioning of the mitotic spindle during cell division has important medical implications and is already used in a number of pharmaceuticals [21, 22]. Most notably, taxanes are a class of chemical compounds that are used in chemotherapeutic drugs to target rapidly growing cancer cells by overly stabilizing their MTs and preventing proper spindle formation, effectively causing the dividing cell to enter apoptosis because of a failure to divide [23, 24]. Targeting and killing cancer cells by perturbing their spindles through the alteration of MT dynamics is a powerful clinical approach to cancer therapy. By better understanding the complex biological system of microtubules, mitotic spindle, and chromosomes, it may be possible to develop better pharmaceuticals to target aberrant cells.

1.1.1 Microtubules and the Spindle

Microtubules [MTs] are cytoskeletal polymers that serve numerous roles within all eukaryotic cells. The polymer is depicted in figure 1.2 and consists of tubulin heterodimers that are approx-

imately 4x5x8 nm and are built from an α-tubulin bonded to a β-tubulin. These heterodimers polymerize along the 8 nm axis of the tubulin in a specific orientation such that the α tubulin of a new tubulin dimer is added to the β tubulin of the previous dimer. The polymerization of tubulin dimers gives the entire MT polymer a polarity such that the end of the MT with an exposed β tubulin is the plus end and the end with the exposed α tubulin is the minus end. MTs are typically more dynamic at their plus ends and are sometimes affixed at their minus end to other cellular organelles, such as the spindle pole bodies during mitosis [2, 3, 6]. Single rows of these polar tubulin dimer strands are known as protofilaments. MTs usually contain 13 protofilaments arranged in a hollow rod shape with an outer diameter of 25 nm, as shown in figure 1.2. The arrangement of the protofilaments typically produces a left hand, three start helix in the MT. MTs have a persistence length of a few mm, where the persistence length is related to the correlation between the tangent angles at each end of the polymer [25, 26]. As the polymer increases in length, the correlation between the orientation of the ends approach zero in an exponential decay, where the persistence length is the characteristic length scale of the decay. When the polymer's contour length is well below the persistence length, it can be approximated as straight. Because most eukaryotic cells are on the order of tens of micrometers in size, MTs are essentially rigid rods due to their length being far below their persistence length.

MTs have critical roles in cell motility, cell trafficking, and cell division. Cell motility, or cell movement, relies heavily on a complex network of two cytoskeletal filaments, actin and MTs [27, 28]. Motility includes crawling, in which the cytoskeletal polymers push on and retract from the plasma membrane of the mobile cell, or a swimming motion that relies on the coordination of the cytoskeletal filaments with motor proteins to beat the cilia and flagella and propel the cell [29, 30]. The MTs also serve as an intracellular highway system that allow motor proteins to walk along them carrying cargo vesicles. This directed motion of vesicles being pulled by motor proteins is visible under a light microscope and has inspired optical trap experiments, in which the vesicle is replaced with a bead that is controlled by a laser trap. The optical trap setup measures the pulling force of the motor protein(s) based on the displacement of the bead [31]. Motor proteins

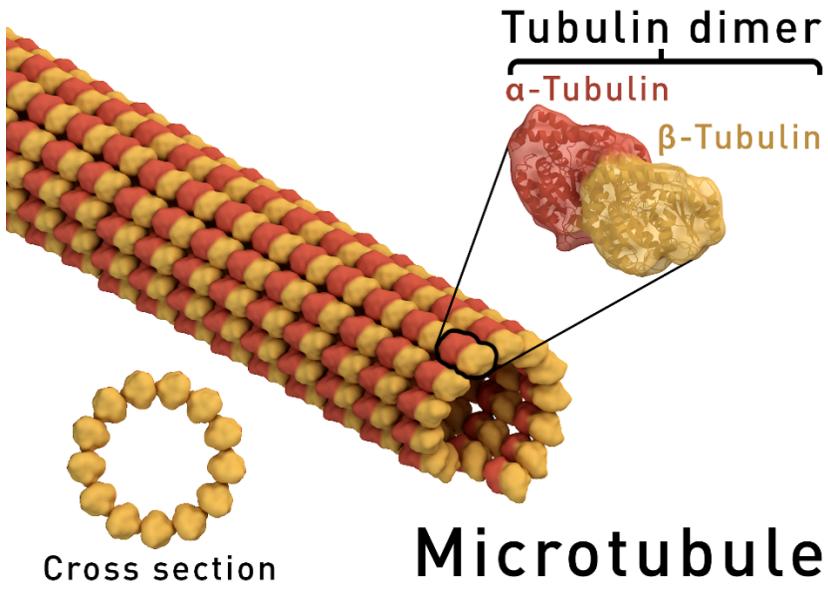

Figure 1.2: This closeup of a microtubule polymer show their hollow rode shape as well as the typical thirteen protofilament ring that comprises the MT lattice. The normal lateral pattern is α to α and β to β, but the underbelly of the MT contains the seam where the lateral tubulin molecules alternate between α and β. The highlighted tubulin dimer is roughly 8 nm in size and is the fundamental subunit of MTs. (Image Credit: *commons.wikimedia.org/wiki/File : Microtubule_structure.png*)

are properly directed to their destinations by the inherent polarity of the MTs and may be either plus-end directed motors or minus-end directed motors.

The role of MTs during mitosis, specifically in their formation of the mitotic spindle and interaction with the chromosomes, that drives the research described in this thesis. During mitosis in fission yeast, MTs nucleate from γ tubulin ring complexes (γ-TuRCs) attached to the surface of sister spindle pole bodies (SPBs) embedded in the nuclear envelope [1, 13]. The mitotic MTs attach to multi-protein complexes, known as kinetochores, that localize on the chromosomes at sites called centromeres. Kinetochores act as adapters between the condensed chromatin and MT polymers [32, 33]. The MT-kinetochore attachment allows movement and alignment of the chromosomes during mitosis. Improper connections between the MTs and kinetochores may lead to aneuploidy, which is highly correlated with certain types of cancers. For example, 90% of solid tumors and 75% of hematopoietic cancers contain aneuploid cells [2, 34]. MTs from sister spindle pole bodies must

connect to sister kinetochores on the chromosome. This arrangement is known as bi-orientation (see figure 1.3) and produces a tension force that may act as a signal and clear the cell to continue mitosis [4, 15]. Upon proper bi-orientation and alignment of the chromosomes into the metaphase plate on the spindle, metaphase is complete and the sister chromatids are severed from each other. The spindle now pulls the sister chromatids to separate ends of the dividing cell. The spatial organization and physical interaction necessary for the chromosomes to be equally divided during mitosis is facilitated by MT polymers.

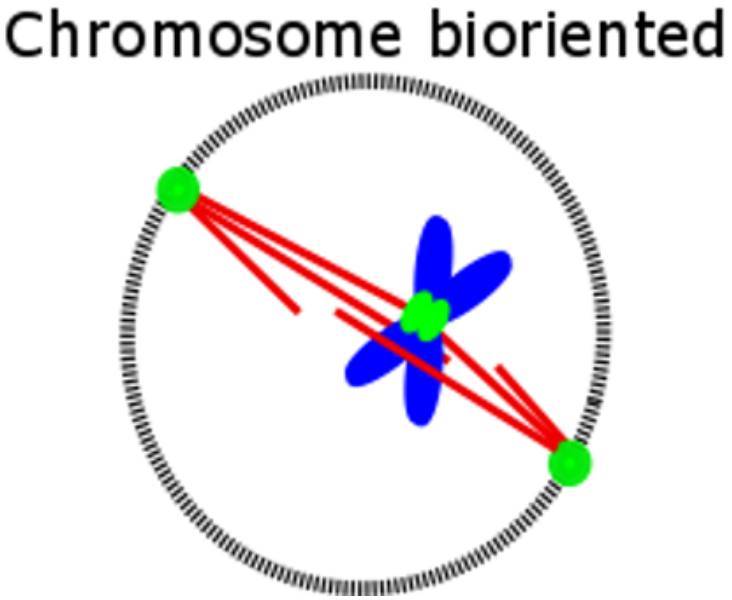

Figure 1.3: This diagram demonstrates the bi-orientation of a pair of sister chromatids. The kinetochore MTs (red) are connected to the kinetochore (shown in green on the blue chromosome). The spindle pole bodies (SPBs) are shown in green embedded in the black nucleus. Biorientation is thought to be essential for the progression of mitosis because the tension balance serves as a signal to proceed with division. (Cartoon Created by Zach Gergely)

Only a subpopulation of the mitotic MTs directly attach to the kinetochores on the chromosomes, properly position them, and physically pull them apart; many mitotic MTs serve as the structural basis for the mitotic spindle [13, 35, 36]. The mitotic spindle is made of interdigitated, dynamic MTs to which motor and cross linking proteins bind. Interdigitation refers to the arrangement of antiparallel MTs, nucleating from different spindle poles, that become associated with

each other by various MT linking proteins, notably ASE-1 [16, 37]. The interdigitated MT-protein structure provides the physical force necessary to partition the chromosomes, because a mutated yeast cell with all other microtubule associated proteins deleted except Ase1 can successfully form a spindle ([16], personal communication). However, the regulation that governs the composition and functioning of the mitotic spindle is not well understood, due to the large number of different components that are involved as well as the large number of redundant parts. The dynamics of the individual MT polymers has been documented as one important regulatory mechanism of mitosis, because when they are significantly altered cells can undergo improper chromosome segregation [3, 16]. The dependence of proper chromosome segregation on MT dynamics intuitively makes sense, because MTs play key roles in chromosome capture, positioning, and segregation: significant change to MT dynamics should affect the cell's ability to segregate chromosomes. In this thesis, I begin to develop a picture of how specifically mitosis relies on MT dynamics and how mitotic MT dynamics depend on various proteins in fission yeast.

Proteins that associate with MTs are known as microtubule associated proteins (MAPs) and serve a variety of functions in the cell. These MAPs can be motor proteins that use the MTs as tracks to walk upon or static proteins that connect MTs together into bundles that exhibit altered dynamics [1, 2, 13]. Bundling occurs because MAPs often have a dimer structure that allows for two distinct MT attachment sites per protein [38, 39]. The ability of the MAPs to bind to multiple MTs causes the protein to act as a spring connecting two MTs into a MT bundle [16]. Bundling of parallel MTs is very similar to the antiparallel bundling (also called interdigitation, described previously) necessary for the formation of the mitotic spindle. MAPs also affect dynamics in ways other than bundling. The multitude of MAPs with known affects on MT dynamics is so extensive that they are referred to as +TIPs proteins because they localize to the more dynamic plus end of the MTs [14]. These proteins change MT dynamics by stabilizing them, increasing their growth speeds, or inducing their shrinkage events through interaction with the tubulin subunits [40]. Because MT dynamics affect the function of the spindle and success of mitosis, it is necessary to consider the role that these proteins may have on these dynamics and, in regards to pharmaceutical applications,

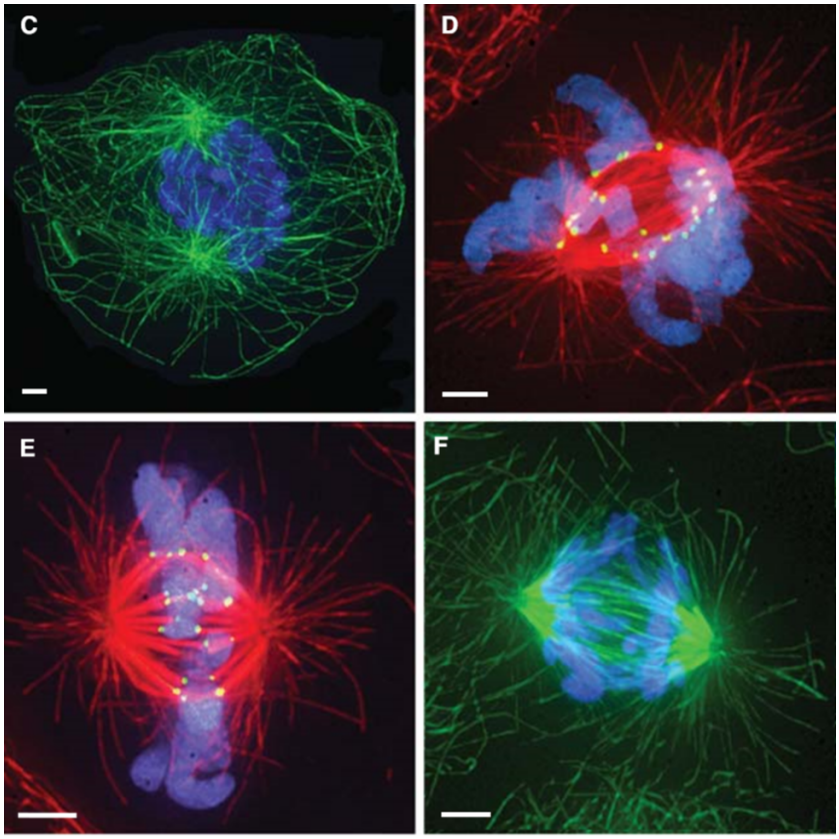

Figure 1.4: These are mitotic spindles from the cell of a rat kangaroo and the microtubules are labeled by immunofluorescence (described later). Scale bar represents 2 microns. (Image Credit: DeLuca lab).

how this physical regulation occurs. To better contextualize microtubule dynamics and my efforts to quantify them, it is necessary to provide a picture of the molecular mechanisms underlying their peculiar polymerization patterns.

1.1.2 Dynamic instability

Microtubules exhibit rapid switches between states of growth and shrinkage in a dynamic pattern known as dynamic instability. Dynamic instability has been an area of active research since its discovery in 1984 by Mitchision and Kirschner [13, 14, 41]. The current biological model explaining dynamic instability is that MTs are polymerized of tubulin heterodimers that contain a GTP molecule attached to both the α and β tubulin proteins. Upon polymerization, these tubulin

heterodimers exhibit a hydrolytic activity that hydrolyzes the GTP β tubulin into a GDP β tubulin form. This hydrolysis event occurs spontaneously and leads to the tubulin heterodimer to prefer a new conformation that exhibits a bend rather than the straight conformation they preferred during polymerization. The conformation switch triggered by the hydrolysis is important because the individual tubulin dimer now prefers to be in a depolymerized state rather than the forced linearity when part of the polymer. The tubulin dimer's self-hydrolytic activity causes them to spontaneously convert from a GTP β tubulin form to a GDP β tubulin form that no longer prefers to remain part of the MT structure, a very peculiar property for a building block. Due to the spontaneity of the hydrolysis event, older tubulin dimers tend to contain GDP tubulin and newer tubulin dimers contain GTP tubulin. This inherent aging of tubulin dimers leads the newer end of the MT, known as the plus end, to contain a "GTP Cap" [13, 14]. The GTP cap preserves the MT structure by preventing the entire polymer from falling apart due to the preferred bent conformation of its older constituent tubulin dimer components. Once the MT loses this GTP cap and becomes fully comprised of GDP tubulin, the individual protofilaments disassemble and the MT rapidly shrinks. The switch from a state of growing to shrinking is known as a catastrophe and the opposite event, a switch from shrinking to growing, is known as a rescue and is much less observed [16, 42]. Lastly, it has been experimentally shown, though not adequately explored, that MTs, especially bundled MTs, exhibit a pause state in which they do not appear to either grow or shrink but maintain a static length over a relatively long period of time [2, 16].

The mathematical model describing dynamic instability requires four parameters: catastrophe frequency (f_c), rescue frequency (f_r), growing speed (v_g), and shrinkage speed (v_s) [43]. The simplified system used to create the model and approximate the behavior of MTs is a set of dynamics rods affixed to a flat plane and spaced apart as to not interact with each other. Because of this restriction on MT interaction, pause states are not described by this model. The original publication described the proposed probability distributions describing whether the MT will grow or shrink given its length and dynamic instability parameters [43], but it also makes a prediction that the average length of MTs can be defined in terms of these parameter values. This prediction

takes the form:

$$< L >= \frac{v_s * v_g}{v_s f_c - v_g f_r} \tag{1.1}$$

This equation is most easily understood if we set the rescue frequency, f_r, to zero, which is admissible because of their very low number of occurrences [16, 42]. Another important aspect to this model is that we will define the catastrophe frequency as the inverse of the average growth lifetime of the MTs, shown as:

$$f_c = \frac{1}{\tau_g}$$

These approximations simplify the average length equation because it leads to the shrinkage velocity term dividing out of the equation, resulting in:

$$< L >= \frac{v_g}{f_c} = v_g * \tau_g \tag{1.2}$$

This length equation shows that the average length, not including rescue events, will be the speed of growth of MTs multiplied by how long they grow for on average. In this context, the rescue frequency and shrinkage velocity act as terms to increase the average length by appropriately considering the ability of MTs to restart growth from a nonzero length. The specific goal of this thesis is to quantify the dynamic instability parameters of MTs in fission yeast during mitosis.

Quantifying the dynamic instability parameters of MTs has not been adequately done in fission yeast during mitosis and is essential for accurate simulations of chromosome segregation. Studying single mitotic MTs has previously been difficult because they are very dynamic and short lived. In larger cells with longer MTs, the spindle is so large and concentrated with MTs and proteins that is is difficult to resolve single MTs. Mitosis in a fission yeast cell, the organism we used in this thesis, only lasts 12 to 24 minutes which makes it very hard to generate significant amount of data pertaining to this phase of the cell cycle. Generating a large amount of data is essential for this work because there exists inherent heterogeneity in the MT dynamics and we aim to produce an averaged set of parameters that reproduce similar activity to the observed behavior. Because the MTs are only 25 nm in diameter and exhibit rapid dynamics, it requires a powerful

microscope to capture the MTs with high enough spatiotemporal resolution as to be able to begin to accurately quantify their dynamics. Previous attempts at characterizing MT dynamics involved *in vitro* MTs, interphase MTs or MTs in a system that used an imaging label that altered the dynamics they were quantifying [42, 44]. In order to generate quality data of mitotic MTs for this project, it is critical to employ modern microscopy modalities and techniques to capture data and quantify dynamic instability in a mitotic cell that exhibits truly biological characteristics.

1.2 Fluorescent Microscopy

Microscopy is an essential to for biological research. Manipulating light in order to peer at smaller and smaller objects has been an essential technique for biologists hoping to understand the fundamental mechanisms of life that occur at a scale indiscernible by the naked eye for centuries [10, 13]. Traditional microscopes rely on the combination of a light source that illuminates the sample, lenses that capture and focus the light, and filters that select for specific properties of the light. Classic microscopy techniques involved exploiting physical properties of light that are different upon interaction with the sample. The change in the light that occurs upon interacting with the sample is used to create a signal that can be filtered and then projected onto our retina or translated by a camera into an image. There are numerous types of microscopes that harness different properties of light in order to visualize the sample. Some of the classic techniques of light microscopy and the properties they utilize are: Brightfield (transmission of light), Darkfield (scattering of light), Polarization (polarization of light), and Differential Interference Contrast (phase of light). These techniques have all been essential to our understanding of biological systems and are still used today to probe the unseen behavior of biological systems [12, 45].

While classic techniques for cell microscopy remain important to biological research, fluorescent microscopy is a relatively new and increasingly popular microscopy modality that departs from the traditional process of illumination and collection with the same light [11, 46]. Rather than exclusively using the alteration of the light upon its interaction with matter to generate signal, fluorescent microscopy explicitly utilizes quantum mechanics and clever labeling techniques to induce

the sample into generating its own light upon stimulation. To be specific, fluorescence microscopy utilizes an atom's ability to absorb and emit a photon of different energies in order to produce images.

Atomic fluorescence is a phenomenon explained by quantum mechanics. The atomic absorption of a photon will only occur if the incident photon exactly matches the energy gap between the excited states of the valence electrons in the atom[11]. Because the energy gap must be closely matched by the illumination light, illumination sources in fluorescent microscopy are either filtered or monochromatic to fit the specific energy gap. A schematic of the quantum phenomenon of fluorescence is shown in figure 1.5 and is known as a Jablonski diagram, named after the physicist Aleksander Jaboski who first depicted the phenomenon of fluorescence with this intuitive diagram [46]. It depicts the absorption of an excitation photon which promotes the electron to an excited energy level. The excited electron quickly (∼picoseconds) relaxes to a local minimum energy level and then eventually (∼nanoseconds) fully relaxes to the global minimum energy level which leads to the emission of a photon in a random direction. The loss of energy due to the vibration is what is known as a Stokes shift and underlies the essential principle underlying fluorescence microscopy: the emission wavelength is different than the excitation wavelength [11, 46].

$$\mathrm{E} = \mathrm{hf} = \frac{hc}{\lambda}$$

$$\Delta E = hc * (\frac{1}{\lambda_{excitation}} - \frac{1}{\lambda_{emission}}) \tag{1.3}$$

Where h is Planck's constant and c is the speed of light.

The energy difference of the light after interaction with the sample allows us to filter the light and image only the light that is emitted from our labeled sample, not the illumination source light.

It is worth highlighting that although fluorescence microscopy differs significantly from classical modalities by implementing labels that cause the sample to emit light of a different wavelength, the techniques employed to make use of this quantum phenomenon and develop the image still rely

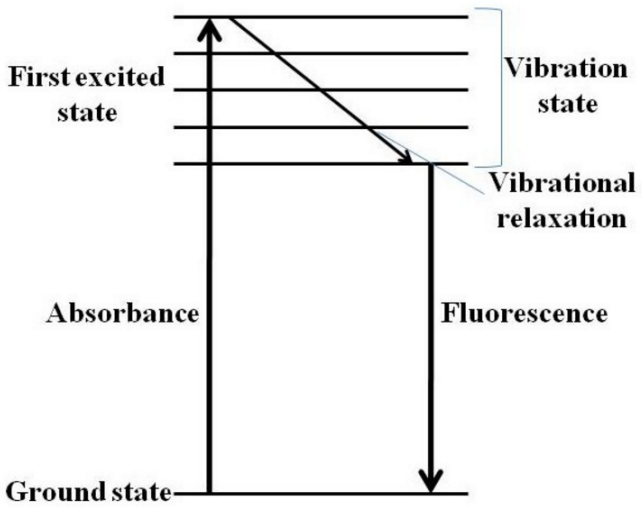

Figure 1.5: This diagram illustrates the physical principal underlying fluorescence. The incoming photon that is absorbed by the atom has energy that matches the energy gap and elevates an electron into an excited state. The excited electron immediately loses energy through vibration and then fully relaxes to the ground state energy level, emitting a photon of lower energy. The difference in energy between the incident and emitted photons underlies the principal of fluorescence microscopy that allows for signal creation. (Image Credit: cnx.org/contents/QisAdlV2@1/The-Application-of-Fluorescence)

on exploiting differences in the physical properties of light. The difference in wavelength allows for the separation of excitation and emission light by the use of a dichroic mirror (see figure 1.6) which allows for the transmission of certain wavelengths and the reflection of others. So, rather than filter the emitted specimen light based on polarization or phase, fluorescence microscopy optics filter based on wavelength. While innovative and useful, this microscopy technique is still hampered by classical constraints, namely the resolution limit of light.

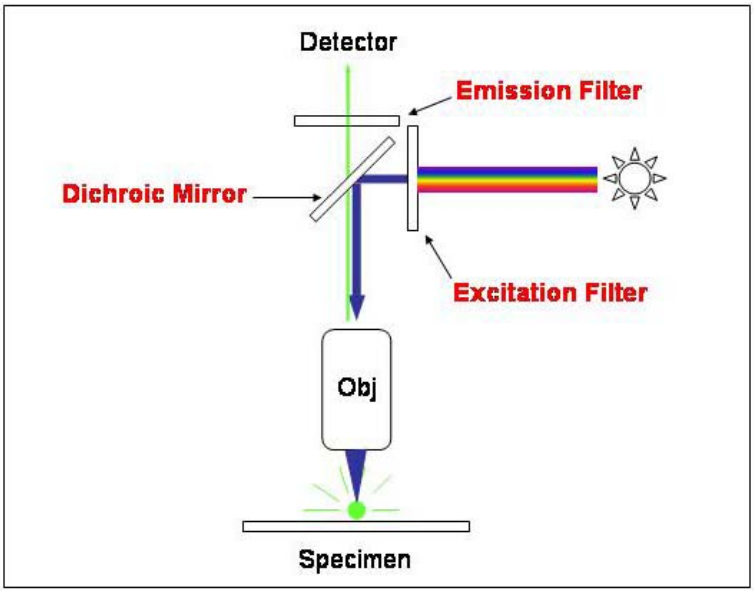

Figure 1.6: This diagram illustrates the basic optical setup of a fluorescent microscope. The emission source can either be broadband (as shown) or monochromatic (laser, not shown). Both excitation and emission light is filtered as to increase the signal produced by the fluorescent sample. The dichroic mirror allows for the excitation and emission light to be separated. (Image Credit: *serc.carleton.edu/microbelife/research_methods/microscopy/fluromic.html*)

1.2.1 Resolution Limits of Light

The resolution limits imposed by the physics of light is an obstacle for cell biologists who wish to use microscopes to observe the functions of life on an increasingly small scale. Resolution is defined as the ability to discern two objects based on a separation of their intensity profiles, as shown in figure 1.7. When the objects become too close to each other they appear as one object and

are described as unresolvable. The resolution limits of light microscopes come from two distinct sources, aberration and diffraction. Aberration refers to the unintended degradation of image quality due to the lenses used in the microscope. The solution to aberration is a technical one, using better lenses, and is not an inherent limit to our resolving capability. However, diffraction is an intrinsic characteristic of light and comes from the fact that photons are electromagnetic waves. Their wave-like behavior means they do not distribute their intensity at a single point on the camera, but rather spread it out over multiple pixels on the camera. The specific shape that a point source will take upon imaging is known as the point spread function and varies depending on the microscope [47]. The diffraction limitation is so fundamental to light itself that the resolution limit is often referred to as the diffraction limit. The diffractive characteristic of light was first described by Abbe and later quantified by Rayleigh in what is known as the Rayleigh criterion, which is the minimal separation distance required to distinguish two objects. The minimal distance is described by:

$$\theta = 1.22 * \frac{\lambda}{D} \tag{1.4}$$

Where θ is the angular separation of the two objects, λ is the wavelength of the emitted light from the two objects, and D is the size of the actual object being imaged. The factor of 1.22 comes from the geometry of the aperture used to collect the light, 1.22 assumes a circular geometry.

The resolution obtainable in an image depends on the wavelength of light collected to form the image, as shown in equation 1.2. The relation of resolution to wavelength has led to microscopy modalities that exploit this, most notably electron microscopy that uses electron beams with a wavelength on the order of half an angstrom, allowing for near atomic resolution of biological structures [48, 49]. However, for live cell imaging, it is desirable to use a light source that is not going to overtly damage the cell and as the wavelength decreases, the energy increases and so does the potential to cause irreparable damage to the sample. This potential damage means that

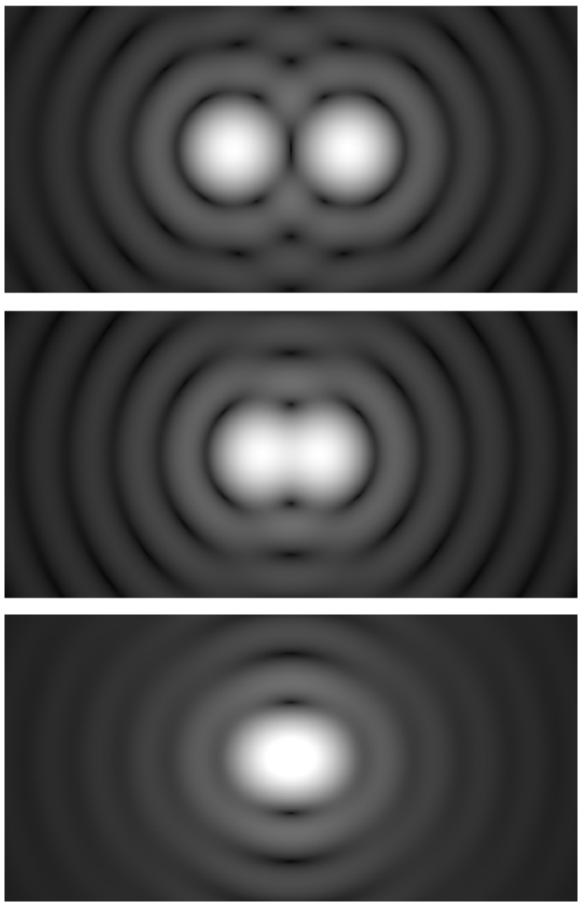

Figure 1.7: This diagram illustrates the idea of resolution. In the top image it is clear that there are two objects present that both display an intensity profile that matches a Bessel function. The second image shows the objects slightly overlapping, but still distinguishable. However, the third image depicts the object when their separation distance is below that of th Rayleigh criterion and thus are indistinguishable from each other. This inability to perfectly resolve objects emitting light limits the cell biologist from being able to visualize the nanometer scale biological structure underlying observed function. (Image Credit: *commons.wikimedia.org/wiki/File* : *Airy_disk_spacing_near_Rayleigh_criterion.png*)

fluorescent microscopy, as well as the classical methods, are limited to roughly ∼250 nm resolution because visible light is the most common illumination light used and has a wavelength between 400-700 nm. The resolution limit of light due to diffraction is continually being challenged by a number of innovative techniques that utilize a combination of better labels, unique illumination patterns, quantum mechanic effects, and computational analysis. These new methodologies are referred to as super resolution microscopy and will have a major impact on biological research and ensure microscopies essential role in it for the foreseeable future [50, 51].

Even though classic fluorescent microscopy resolution is limited to the Rayleigh criterion, advances in the field have allowed it to provide unprecedented perspective on the cellular scale. Two significant progressions in biological imaging with fluorescence are using genetically encoded proteins to label specific molecules of interest and ingenious fluorescent analysis techniques to probe activity that cannot be resolved.

1.2.2 Fluorescent Proteins and Methods

Fluorescence in cell biology has greatly impacted current research and is continually growing as an indispensable microscopy tool. The ability to genetically encode fluorescent proteins into the cell of interest has revolutionized biological research by permitting a powerful and consistent method to label proteins of interest *in vivo* with unprecedented precision. Prior to fluorescent proteins, labeling a molecule of interest with a fluorescent probe required inserting a foreign fluorescent molecule into the cell. The first experiment that utilized fluorescence was performed by Ellinger and Hirt in which they fed a cell a fluorescent molecule and then exposed the cell to incident light that caused the molecules to emit light and the cell to glow [10, 11]. However, being able to specify which molecules emit light is essential for properly understanding what the images depict. Precision fluorescent labeling occurred with the development of fluorescent antibody staining in the 1940s [11, 52]. Antibodies are natural products of the immune system and are synthesized in order to specifically interact with and disable foreign molecules viewed by the cell as a threat. Researchers co-opted this targeting ability and developed antibodies affixed with a fluorescent molecule that

could seek out and bind proteins of interest to make them apparent in an image. This technique is known as immunofluoresence and is still used today to precisely label sub-cellular structures (see figure 1.4).

The discovery and development of fluorescent proteins, known as fluoraphores, has improved the utility of fluorescent microscopy because it allows for accurate, genetically encoded labeling. The first widely studied and used fluorescent protein came from the jellyfish, *Aequorea victoria*, and is known as green fluorescent protein (GFP) [53, 54]. Unlike immunofluorescence which requires the insertion of foreign antibodies into the cell to attach a fluorescent probe to the molecule of interest, fluoraphores are encoded in the DNA of the cell of interest and allow for a more natural probe that is a structural part of the protein of interest. However, the direct incorporation of the label into the structure of the protein is not ideal because fluorescent labels can be comparable in size to the protein of interest. For example, the mCherry label we use to label the tubulin dimers in this thesis is approximately a fifth of the weight as the tubulin protein alone. The added weight of the label surely affects the behavior of the labeled protein and must be considered when planning experiments or comparing results.

Progression in precise gene editing and protein design complements the effectiveness of fluorescent labels. Gene editing enables biologists to specifically label a species of protein *in vivo* with a fluorescent protein by inserting the raw DNA sequence that encodes the protein into the gene of interest in the organism. The classic gene editing method inserted a DNA fragment encoding a fluorescent tag into a genome by using zinc fingers, which are proteins that interact with specific DNA sequences; but modern research has discovered the new CRISPR-Cas9 system from the immune system of bacteria which enables more precise genetic splicing [14, 55]. Developments in protein design have enabled researchers to modify the GFP in order to manipulate the quantum properties of the fluorescent probe such that they can absorb and emit light of different wavelengths or under different conditions (see fig 1.8) [53, 56]. The effort of expanding the library of fluorescent proteins and understanding their utility resulted in a Nobel prize in 2008. Fluoraphores will continue to impact biological research and allow for a deeper studying of life on a sub-cellular scale with minimal

perturbation.

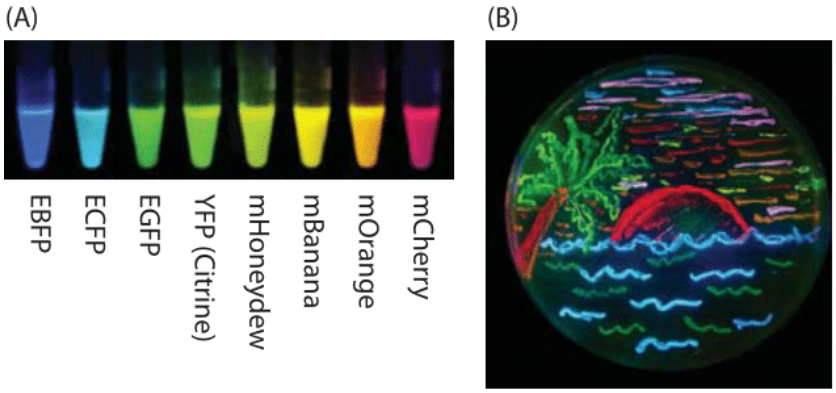

Figure 1.8: This diagram illustrates the diversity of fluorescent proteins. Figure A shows the spectrum of colors that are possible to encode in a cell of interest with a fluoraphore. Figure B demonstrates the power and control of fluorescent proteins by depicting a beach scene created by only bacteria and fluorescent proteins. (Image Credit: www.tsienlab.ucsd.edu/Images.htm)

Fluorescent proteins enabled scientists to use a number of innovative techniques to probe beyond the diffraction limit of light. These techniques fall into roughly two categories: bleaching and energy transfer. Bleaching describes the phenomenon of the fluorescent signal gradually becoming dimmer and dimmer as it is imaged over time [11]. Bleaching is explained by the inability of the excited electron to relax and emit a photon. Two ways this may occur are the spontaneous loss of the excited electron in the fluorescent atom to either a more electronegative atom nearby or a change in conformation of the protein itself into a form that no longer allows fluorescence. With the excited electron removed from the atom before it can relax, no photon will be emitted and thus our signal on the camera will decrease. While normally an effect that is minimized during imaging, fluorescence recovery after photobleaching (FRAP) and fluorescence loss in photobleachng (FLiP) utilize bleaching as a means to determine diffusion and kinetic rates [57, 58, 59, 60]. These techniques rely on using a high powered laser to bleach the sample in a small diffraction limited sized spot. The intensity of the bleached spot gradually recovers because the bleached molecules are replaced with unbleached molecules in FRAP, or that the bleached molecules are taken up and distributed into a multi-molecular complex with a corresponding decrease in signal as bleached

subunits replace unbleached subunits in the structure of interest (in FLiP). Both of the intensity vs time curves produced by this exchange with bleached and unbleached probes can be fit to extract out diffusion and half life times. These methods represent innovative techniques that allow for the quantification of physical parameters that are not resolvable by the microscope.

I will further elucidate the theoretical underpinnings of FRAP because I utilized it in this research project to quantify the dynamics of unresolvable MTs in the mitotic spindle. Researchers first utilized photobleaching to quantify the mobility of proteins in the cell membrane to establish the fluid mosaic model [14, 59]. A simplified explanation of photobleaching analysis is that it attempts to fit the intensity recovery profile with a function that has an interpretation pertaining to some physical characteristic about the bleached molecular subunit. The expected recovery profile that is fit in a FRAP procedure takes the approximate shape shown in figure 1.9 where the nomenclature of mobile and immobile fractions pays tribute to the membranous origins of FRAP. The notion that certain molecules are stationary and thus prevent full recovery in intensity makes sense in a membrane context; but a better explanation of why recovery is not complete is that in the process of bleaching the sample, many proteins are either permanently destroyed or altered which leads to a lowered intensity signal. The half life value, designated as $t_{1/2}$ in figure 1.9, is the time it takes for half of the new maximum intensity to be reached, implying that half of the mobile bleached fraction has been exchanged with unbleached molecules. In the next chapter I will describe the specific FRAP procedure I used to quantify the turnover rates of polymerized tubulin in the early mitotic spindle.

Energy transfer is also utilized to probe the separation distance of two molecules with an accuracy well below that of the diffraction limit [61, 62]. The energy transfer technique utilizes the quantum effect of atoms absorbing and emitting photons of a specific energy in consecutive stages, as shown in figure 1.10. The key is to label two molecules that are believed to interact with different fluorescent tags. These two fluorescent tags must undergo Forster Resonance Energy Transfer (FRET) in which one of the tags, the donor, is excited by the illumination source and then emits light that is absorbed by the other tag, the acceptor, which then emits a photon of a

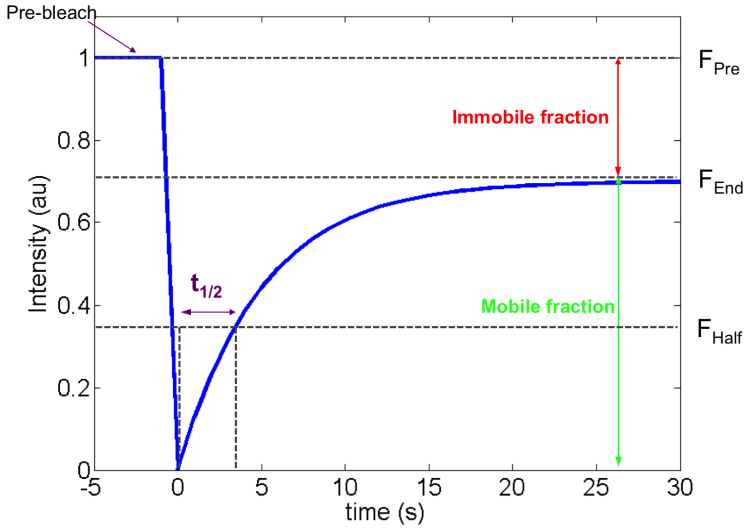

Figure 1.9: This plot depicts a sample intensity curve measured in a FRAP experiment. The initial intensity steeply drops upon the bleaching event an then gradually recovers to a new maximum value. The new maximum value is lower than that original because there exists an immobile (denatured) fraction of proteins that will never fluoresce after bleaching. The recovery portion of the curve can be fit in order to extract the half life, $t_{1/2}$, of the molecule of interest. The half life indicates the time it takes for half of the mobile bleached molecules to be replaced with unbleached molecules. This type of experiment allows for the quantification of chemical kinetics which are normally irresolvable on a microscope. (Image Credit: http://aicblog.janelia.org/wp-content/uploads/2014/09/FRAP-Fig-1.png)

longer wavelength than either illumination source or donor. The FRET method is essentially two rounds of fluorescence where we utilize one fluorescent probe to act as the illumination source for another. This energy transfer will only occur if the tagged molecules are within nanometers of each other because the efficiency of this energy transfer is proportional to $\frac{1}{r^6}$ [63]. The rapid attenuation in transfer efficiency means that observation of the acceptor tag's fluorescent signal implies that the two molecules are interacting with each other. The FRET technique is powerful and has led to knowledge of the cellular landscape at a scale unresolvable by normal light microscopy.

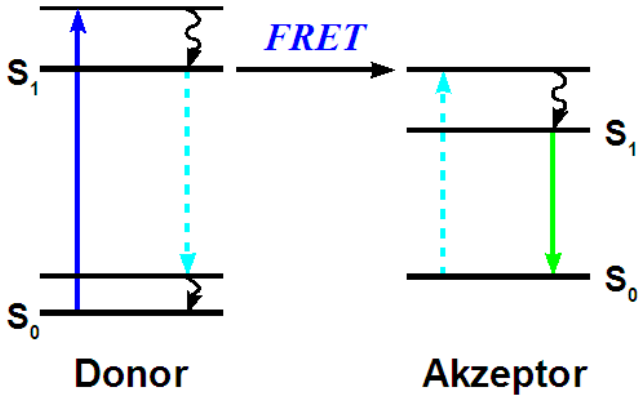

Figure 1.10: This diagram illustrates the process of Forster Resonance Energy Transfer (FRET). This process involves the transfer of energy from one fluorescent molecule to another. This is done by matching the emitted energy of the donor to the excitation energy of the *Akzeptor* (German for acceptor). This allows probing of sub diffraction limited distances because this energy transfer only occurs when the donor and acceptor are near each other, where 50% transfer efficiency occurs at the Forster distance, a unique distance for each donor/acceptor pair that is on the order of ∼1-10 nm. So we know the molecules are within nanometers of each other if we see the signal from the acceptor molecule. (Image Credit: de.wikipedia.org/wiki/Datei:FRET-Jablonski2.png)

1.3 Fission Yeast as a Model Organism

Fission yeast, formally known as *Schizosaccharomyces pombe*, are an indispensable organism for cell cycle and mitosis research due to their low maintenance, quick generation time, low number of chromosomes, and genetic similarity to higher Eukaryotes. The fission yeast are a unicellular Eukaryote that are distant cousins of *Schizosaccharomyces cerevisae* which is commonly called budding or bakers yeast. Fission yeast are cylindrical with hemispherical ends and are roughly 4 μm in diameter and 7-14 nm long (see figure 1.11). They undergo a closed mitosis, meaning their nucleus does not degrade during division. Cell division of fission yeast is visible on a light microscope because of the fission event that leads to two daughter cells [2]. The use of fission yeast as a model organism began in the 1950s as a tool to probe the stages and regulations of the cell cycle, shown in figure 1.1. Researchers were able to observe and measure physical properties of the cell, such as length, as well as manipulate the genetics [64, 65, 66].

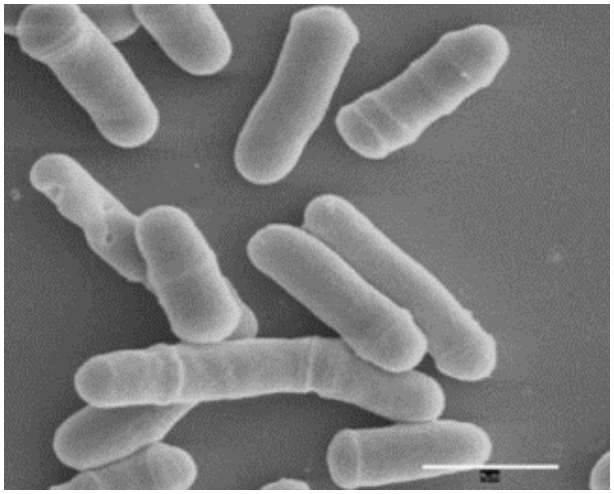

Figure 1.11: These are images of fission yeast taken with a scanning electron microscope (SEM). (Scale bar represents 5 microns) (Image Credit: commons.wikimedia.org/wiki/File:Fission_yeast.jpg)

In the 1970s, Paul Nurse and others furthered the importance of fission yeast as a model organism by connecting the genetic manipulation techniques to the cell cycle work, essentially creating a system that allowed for both perturbations and corresponding measurements [66, 67].

This work led to the discovery of critical cell cycle control genes known as cyclin dependent kinases (CDKs) that regulate the cell cycle through coordinated phosphorylation events, a mechanism that is conserved in all known Eukaryotes and resulted in a Nobel Prize in 2001 [68, 69]. With the detailed knowledge of the fission yeast's cell cycle and genome editing methods combined with technological progression in microscopy and computational techniques, the setting is appropriate to begin to use this organism to explore further the molecular and physical basis of mitosis.

1.4 Looking Forward

The remaining chapters of this thesis deal with the specific experimental methods and computational analysis I implemented to better quantify the dynamics of MTs in mitotic fission yeast cells. Chapter 2 discusses the experimental microscopy setup used in order to image the yeast as well as the numerous computational tools developed in order to automate the analysis of these micrographs. Chapter 3 reflects on the progress made in this project as well as discusses possible follow up projects to complement and extend the work described in this thesis. Although this research did not completely elucidate the complex interplay between individual MTs, the mitotic spindle, and the chromosomes, it has developed tools that will be useful in extracting the necessary physical parameters from images; a critical step for simulating and, ultimately, understanding mitosis.

Chapter 2

Biological and Computational Methods

Research efforts to understand the mechanisms of mitosis have benefited from both biological and computational advances. Fluorescent proteins and imaging allow scientists to label and observe individual components of the mitotic spindle complex, the essential biomechanical machine to divide sister chromatids. Advances in genetic engineering permit scientists to perturb individual spindle components with specificity and then record their corresponding macro effect on chromosome segregation. Combining these methods with advances in computational techniques makes it possible for scientists to ask, image, model, simulate, and ultimately answer questions about the underlying function driving mitosis. Computational techniques that analyze microscopy images in order to quantify physical characteristics of the sample provide an innovative method to extract meaningful data from images. Measured physical characteristics are then implemented in mathematical models of the biological system as known parameters and allow for the simulation of biological systems. These simulations allow researchers to perform experiments that are not possible *in vivo* and garner meaningful statistics to elucidate biological trends unnoticed otherwise. The combination of improved biological imaging, powerful image analysis algorithms, and new simulative methods allows biologists to ask questions from an unexplored perspective.

I have utilized this collection of biological and computational tools in order to better quantify the dynamics of mitotic microtubules in fission yeast. In regards to experimental bioimaging work, I have assisted in developing a novel genotype of fission yeast and an imaging protocol that together allow for a prolonged look of cells during early mitosis, prior to the formation of the bipolar spindle.

We call this state a monopolar spindle because the cell is stalled in prometaphase with spindle pole bodies nucleating MTs but unable to separate from each other and form a bipolar spindle. I also performed bleaching experiments on both monopolar and bipolar spindles to quantify the microtubule kinetics and how they may differ in the two states. My computational research focused on image analysis of the microscopy data. Specifically, I have developed image analysis software, both a semi-automated and fully automated method, that can accurately measure microtubule length with sub pixel accuracy. I have began to use this software to quantify dynamic instability parameters. I also authored a kinetic Monte Carlo simulation of the monopolar spindle state to better tune dynamics parameters as well as to quantify the performance of the image analysis software. My efforts have resulted in the development of essential analysis tools and imaging protocols to analyze mitotic microtubules in fission yeast and have better quantified their microtubule dynamics, parameter values necessary for developing an accurate model of mitotic spindle formation.

2.1 Developing a "Wild Type" Fission Yeast Strain

We developed a strain of fission yeast that allows for a prolonged look at early mitosis in cells with fluorescently labeled tubulin, a critical step for gathering data on mitotic microtubule dynamics. Creating a strain of yeast that is stalled in early mitosis was essential because this phase of the cell cycle occurs in minutes in unaltered cells. The brevity of mitosis makes it impractical to quantify the mitotic MT dynamics in normal yeast because each cell only provides a small amount of data in a transient state that is difficult to image. Because of the heterogeneity of the MT dynamics, large averaged parameter values are desired in order to produce representative simulations. By using a strain of fission yeast with a temperature sensitive protein, we were able to synchronize a large number of cells to be in the relevant phase of the cell cycle and image their fluorescently labeled mitotic MTs indefinitely. We have used this basis strain to quantify the dynamics of MTs as well as to serve as a foundation for a strain library with additional genetic perturbations.

In order to stall the fission yeast in mitosis, we implemented a temperature sensitive allele

of the kinesin-5 protein known as cut7 in fission yeast. A temperature sensitive allele produces a gene product that exhibits distinct levels of functionality within a biologically relevant temperature range. We utilized a cut7-ts allele that did not function at 37° C in order to arrest the cells in early mitosis [70]. This cell cycle block occurs because the cut7 protein normally binds antiparallel MTs and slides them in antiparallel directions, beginning MT interdigitation that creates an initial separation between the spindle pole bodies. Biologists believe that this initial separation is necessary for bipolar spindle formation because the increased distance of the spindle pole bodies allows for an increased number of interdigitated MTs, the structural backbone of the spindle [16, 36]. With the spindle pole bodies unable to separate because cut7-ts is nonfunctional, the cells are arrested in early mitosis for as long as the cells are maintained at 37° C and still healthy.

We visualized the MTs in the stalled cells with the fluorescent protein, mCherry, attached to the alpha tubulin II molecule that, with beta tubulin, comprises a subpopulation of tubulin dimers present in MTs. Fission yeast contain two variations on the alpha tubulin protein, alpha tubulin I and II, and by using only one as a label we are effectively lowering the number of altered tubulin dimers present in are MTs. Fluorescent labels are known to affect the dynamics of MTs and makes choosing an appropriate label difficult. An ideal fluorescent tag will provide a large signal while not altering the normal dynamics of the MTs. However, this ideal label does not exist and this has led us to settle on employing a somewhat dim mCherry label that allows visualization of MTs with minimal functional perturbation. To ensure that the mCherry only minimally affected the MTs dynamics, the strain of fission yeast that we use produces enough mCherry protein to label $\tilde{8}$% of all alpha tubulin present [16]. The low labeling level means that many of the tubulin dimers are not structurally altered and can be assumed to function in an unperturbed state. Using a low level of fluorescent label to preserve the integrity of our system has come at the cost of lowering the intensity signal measured by our camera. Low signal is a major challenge for the image analysis portion of this project, to be described later. However, by constantly working to improve our image quality, we have been able to increase the signal to noise ratio significantly and improve our ability to analyze the data present in the micrographs.

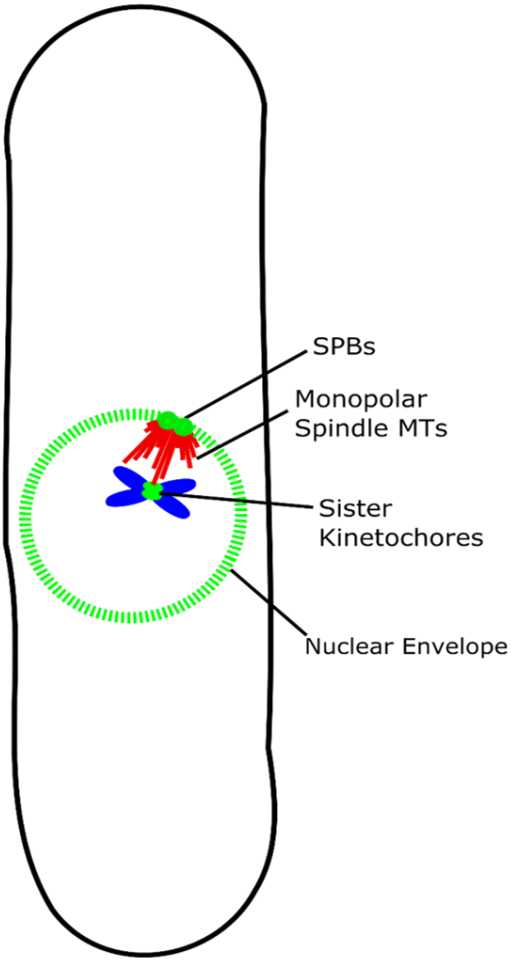

Figure 2.1: This cartoon represents the cut7-ts monopolar fission yeast system that we image on the microscope. The monopolar spindle consists of two co-localized spindle pole bodies (SPBs) nucleating MTs in prometaphase. We have developed different yeast strains in order to label and observe all of the annotated parts of this cartoon to get a fuller picture of mitosis. Our "wild type" strain contains only the cut7-ts allele and an mCherry label on the MTs. (Cartoon by Zach Gergely)

2.2 Imaging Protocol

In tandem with creating a strain of yeast that allows for a prolonged look at the dynamics of mitotic MTs, we developed a corresponding imaging protocol that maintained the monopolar spindle state by keeping the yeast at 37° C throughout the entirety of the imaging session. Our focus on maintaining a constant temperature led to a number of distinct adaptations relative to a typical sample preparation. The key features of prepping the temperature sensitive fission yeast in order to image them in a monopolar state begins with placing them in an incubator set at 37 °C roughly 2-4 hours before they are actually imaged. The incubation period produces a large number of cells that have entered mitosis and become stalled. We then prepare a microscope slide and coverslip inside of the incubator, working in small shifts as to keep the internal temperature of the incubator near the desired 37°C. In order to adhere the yeast cells to the coverslip and prevent them from diffusing during imaging, we lay down lectin proteins that interact with the exterior of the yeast cell and hold them still. After the yeast are affixed to the coverslip and locked in early mitosis, we quickly transfer them from the incubator onto the microscope and assemble them underneath a microfluidic chip that maintains the desired temperature. The commercial microfludic temperature control system we use, named Cherrytemp, allows us to accurately maintain the temperature on the microscope as well as rapidly switch the cells between two preset temperatures. Switching between temperatures enables us to image a monopolar spindle indefinitely and then switch the temperature to the natural 25°C and continually image the cell as it transitions from the monopolar state into the bipolar spindle. The combination of the incubator, rapid transfer, and microscope temperature control unit allows us to image the exact part of the cell cycle that we desire for this project.

We imaged the fission yeast's mitotic spindles with a Nikon inverted Yokogowa spinning disc confocal microscope. This microscope utilizes the set up shown in fig 2.2 that depicts the confocal principle of using a pinhole to block the out of focus emission light. This differs from the classic brightfield method where all of the light emitted from the sample is collected. Filtering out of focus emission light leads to improved resolution in terms of the depth of the sample because the pinhole

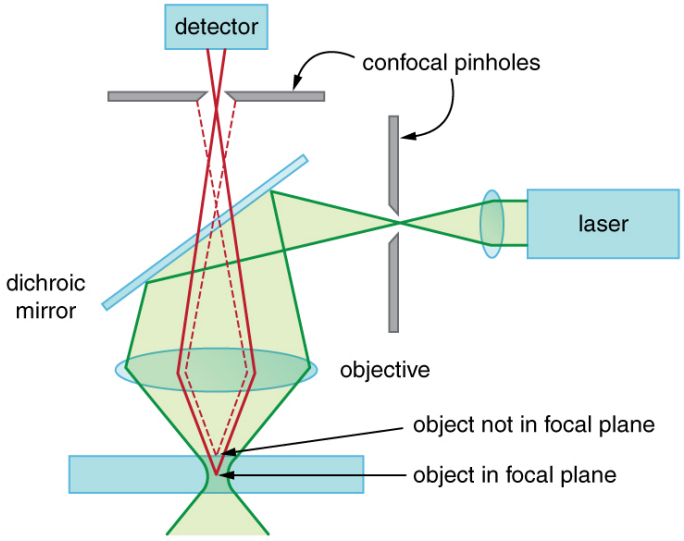

Figure 2.2: This schematic depicts the underlying optical setup of a confocal microscope. We can see that the illumination with the green light induces fluorescence of red light. The dichroic mirror reflects the green light and transmits the red light. After the green and red our separated, as in a normal fluorescent microscope, the red light is further filtered by the pinhole in front of the detector. This pinhole blocks out of focus light and ensures that only one sample depth is being visualized on the camera, allowing for 3D sectioning of biological specimens. (Image Credit: archive.cnx.org/contents/4cfd3c2d-dad1-4133-8dae-0c321a6577a4@1)

blocks light that is not coming from a specific depth within the sample. Confocal microscopes permit 3D sectioning of a sample because of the pinhole filtering. The Yokogowa spinning disc is a technological improvement on the classic confocal schematic by replacing the pinhole before the detector with a Yokogowa spinning disc that has specifically spaced pinholes with microlenses that rotate at a specified frequency and focus light to pixels on the camera [71]. The microlenses on the pinhole collect and focus more light onto the camera which improves the signal from the sample. The spinning disc is a parallelization of the confocal imaging technique and allows for quicker image acquisition because we can illuminate multiple place on the sample simultaneously. This microscope enabled us to acquire images of the mitotic yeast cells with high enough spatiotemporal resolution as to capture the dynamics of the MTs (see figure 2.3). For a series of image stacks that contained 7 separate z planes we acquired a time resolution of $\tilde{1}.8$ seconds per stack. The technical progression of the preparatory protocol combined with the powerful microscope resulted in the acquisition of meaningful dynamics data of mitotic MTs in fission yeast.

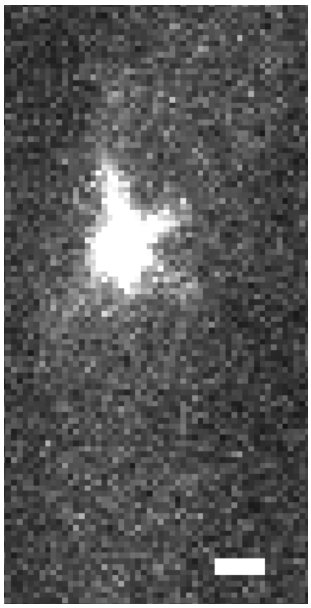

Figure 2.3: This is a sample image of a monopolar spindle. The α-tubulin is labeled with an mCherry fluoraphore and the cell is stalled in early mitosis due to the cut7-ts allele. The spindle pole bodies are thought to be co-localized in the center of the fluorescent mass. Scale bar is 1 micron

2.3 Other Genotypes

Other than the previously described "wild type" strain of fission yeast we created with the cut7-ts and mCherry alpha tubulin label, we produced a series of derivative yeast strains by crossing our basis strain with strains that contained various protein deletions or additional structures labeled. We constructed 40 unique strains of fission yeast that are the foundation of a strain library that will be used to understand how the multitudes of molecular players present interact with each other during mitosis. The strains will complement my effort to better understand mitosis because they will allow us to quantify how various mutations affect the MT dynamics and spindle formation. Figure 2.4 depicts a collage of spindle phenotypes in various mutants and shows how different the monopolar spindles appear based on which MAP is deleted. Connecting MT dynamics to specific MAP function in order to develop a model for how the complicated network of MTs and proteins come together to form the spindle and accurately divide the replicated chromosomes is beyond the scope of this research project, but the creation of a strain library that allows extended observation of how different protein deletions affect the dynamics of mitotic MTs and spindle formation is an important first step towards that ultimate objective. The possible future uses of these other genotypes is further discussed in chapter 3.

2.4 Computational Techniques

With the protocol for imaging mitotic cells established, I will now describe the various computational techniques used to extract biological understanding from the micrographs. The computational efforts that I undertook to analyze the data fall into two general categories: image analysis and simulation. I will first describe the image analysis methods implemented to quantify the dynamics of mitotic MTs, both direct measurement of resolvable MTs as well as analyzing intensity recovery in bleaching experiments to quantify tubulin turnover in unresolvable MTs. I will then describe a kinetic Monte Carlo simulation I wrote to model the monopolar spindle state and to benchmark the performance of the image analysis software. My computational work has led to the

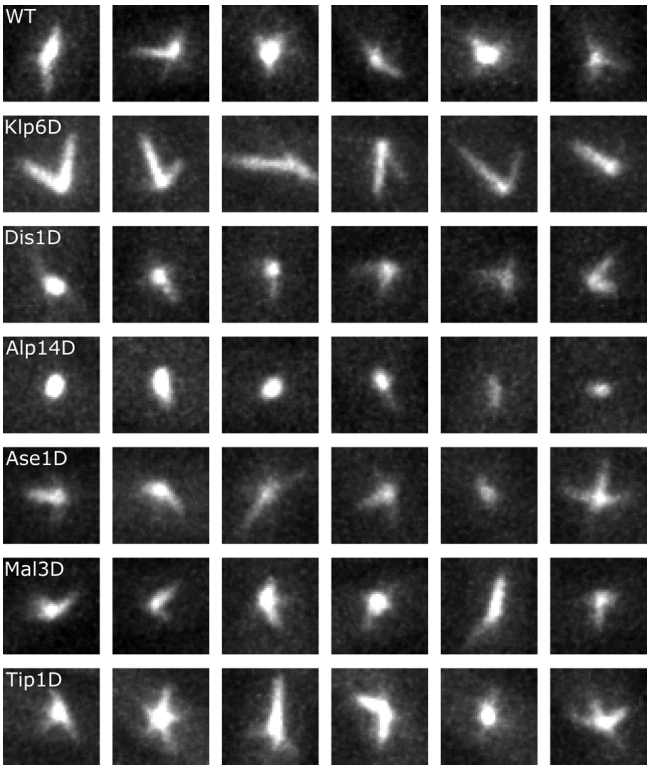

Figure 2.4: A collage of various Microtubule Associated Protein (MAP) deletion strains in fission yeast. The name for each row correspond to the MAP that is deleted. The columns show representative images of each phenotype. Various protein deletions lead to different monopolar spindle profiles.

quantification of MT characteristics in early mitosis as well as the development of image analysis tools that may be applicable in a broad range of contexts.

It is important to note that all of the image analysis work has been done on two dimensional images. Although the acquisition of the data occurs by taking z-slices, I project the maximum intensity pixel from each z column into a two dimensional image known as a maximum intensity projection. A future goal of this work will be to analyze full three dimensional image stacks. I discuss the importance and practicality of three dimensional analysis in the third chapter of this thesis. For this chapter, all references to images and computational methods should be assumed to be restricted to two dimensions unless otherwise stated.

2.4.1 Feature Detection and Tracking

Algorithms designed to automatically detect and track objects in biological images are a relatively new area of study that has critical importance in the analysis of microscopy data [72]. The field of automated image analysis has mostly developed in regards to non biological applications, mainly facial recognition and handwriting interpretation [73, 74]. Unfortunately, many of these current image detection algorithms are only able to function properly if there is a high signal to noise ratio or a spatial organization known *a priori*. This is not an issue for macroscale, ordered features such as handwriting and faces, but is a significant constraint in applying these algorithms to noisy images of complicated biological systems. Adapting and extending current feature detection software so that it may be implemented to automatically process micrographs will permit high throughput image analysis of biological samples. As previously described, the technological progressions in microscopy are allowing imaging on an unprecedented scale. This increased resolution is leading to the visualization of many more molecules, either individually or in aggregate. It is critical to develop software that can identify and follow these molecules throughout an image series in order to determine trends in localization and behavior and to understand how these phenotypes are linked to physical or genetic perturbations. The ability to completely mine the useful biological data buried within an image is a meaningful achievement on the horizon.

In my own research, I worked towards developing software to measure the lengths of MTs and quantify their dynamics in mitotic fission yeast cells. The general algorithmic outline used for achieving this result is: identify mitotic cells in a field of view, quantify the lengths of MTs present in the selected cell, and link detected MTs across frames of the image series taken over time. This procedure results in length vs time data for individual MTs in imaged mitotic cells. My efforts resulted in two distinct software implementations to accomplish this task, one being semi-automated and the other being almost entirely automated. Each measurement technique has different benefits and I will now describe their function and results.

2.4.1.1 TipTracker

I utilized the TipTracker software that was originally developed in the Odde lab at the University of Minnesota [75, 76]. This software had previously been used to measure the location of tips of polymers in mammalian cells with sub pixel accuracy. The tip detection occurs by the user identifying the relevant area in the image and fitting the MT intensity profiles with the theoretical intensity profiles that describe the MT tip. The specific algorithm follows as:

•Identify MT

This step consists of the user inputting two clicks along the axis of the MT, with the second click being nearer the tip. This input serves to define the region of interest as well as the directionality of the MT.

•Identify MT Backbone

This step takes the identified two points on the MT and performs line scans 5 pixels long perpendicular to he axis of the two input points. The maximum pixel found in each of the line scans is marked. A linear line is then fit through all of the maximum pixels, and this is the estimation of the MT between the two selected points.

•Identify MT Tip

With a line approximating the MT between the two points selected, we can now extrapolate the tip position. This approximation is done by following the intensity profile along the estimated MT and

noting when the intensity value is at a full width half max value (FWHM). This point is selected because we know the intensity profile of the MT tip will be approximately Gaussian, and so the FWHM location serves as an approximation to where the MT stops and background begins. A representative example of the software is shown in figure 2.5.

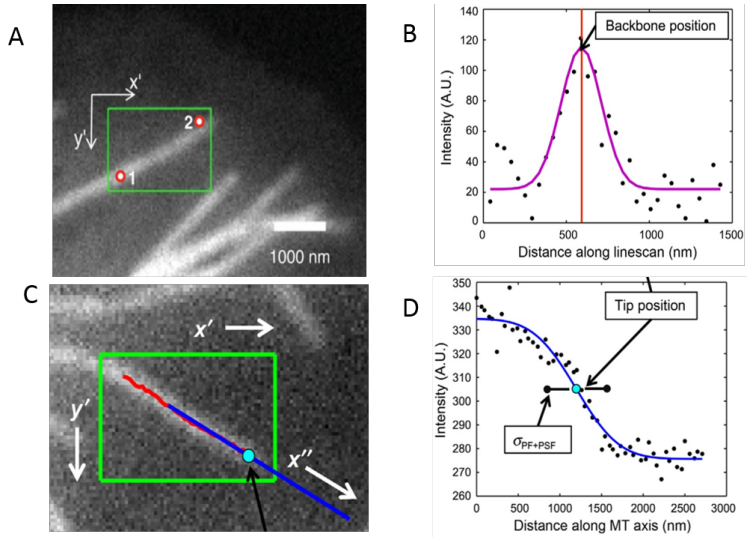

Figure 2.5: These images summarize the function of the TipTracker algorithm. Panel A depicts a sample image in which two points, labeled 1 and 2, have been selected by the user. Panel B depicts a representative intensity profile when taking perpendicular line scans to the MT, the peak of the profile is kept as an MT backbone position. Panel C shows both the raw MT backbone line in red and the linear fit to that line in blue. The blue line is used to extrapolate tip position. Panel D shows a representative intensity profile along the blue line towards the tip. The final tip position is determined to be where the full width half max value occurs. This algorithm allows for sub pixel determination of the MT tip position.

The TipTracker procedure enables us to determine the position of the MT tip in an objective manner based on the intensity profile near the tip of the MT. However, in its original form, the software could not measure multiple tips at once, connect multiple tips throughout a series of images, or identify a nucleation site. I modified the software with these features which made it possible to not only determine the tip of a single MT, but to quantify the length of multiple MTs throughout a movie and generate dynamics data. These modifications can be summarized as:

•Detect Multiple MTs

Detecting multiple MTs in a single frame was a critical development because most of the observed

monopolar spindles have multiple MTs present. I applied this alteration by modifying the original TipTracker code to allow for all data to be stored in vectors with a length matching the number of MTs present in the given movie. I then implemented a loop over all frames where each frame allowed the user to provide two clicks for each MT present. If an MT was not present, its length for the frame was set to 0.

•Connect MTs Through Image Series

My extension of the code to account for following objects through multiple frames resembles the most primitive tracking algorithm imaginable - a fully manual specification of which object is which in consecutive frames by the user. Although somewhat subjective, our time resolution was fast enough such that it is possible to connect arms between consecutive frames because MTs are often spaced far enough apart and do not display large angular displacement. I implemented this modification with a preliminary interface where the user would label all of the arms that appear throughout the movie. Although crude, this method allowed us to track multiple MTs throughout an entire image sequence.

•Determine Location of Nucleation Site

The original TipTracker software had no capability to locate the origin of the polymer whose tip is being detected. The ability to quantify the lengths of the MTs requires knowledge of the tip as well as knowledge of where the MT begins. Based on the biological knowledge of the monopolar spindle system, we knew the MTs nucleate from spindle pole bodies (SPBs) that are unable to separate due to the cut7-ts allele described previously. So, to approximate the location of this monopolar center, we allowed the algorithm to calculate the coordinates for the centroid of the intensity profile of the labeled monopolar spindle. We used the centroid coordinates to approximate the nucleation site of the MTs and were then able to calculate length of the MT by determining the linear distance between the tip location and the nucleation site.

I successfully modified the TipTracker software to measure the dynamics of mitotic MTs [16]. This method resulted in the histograms shown in figure 2.6. The results of this effort led to parameter values that were used in a full mitotic spindle formation simulation. Connecting the

results of image analysis to a mathematical model in order to successfully simulate the construction of a macromolecular biological complex is an example of modern interdisciplinary biological research that promises new experimental avenues and pursuits.

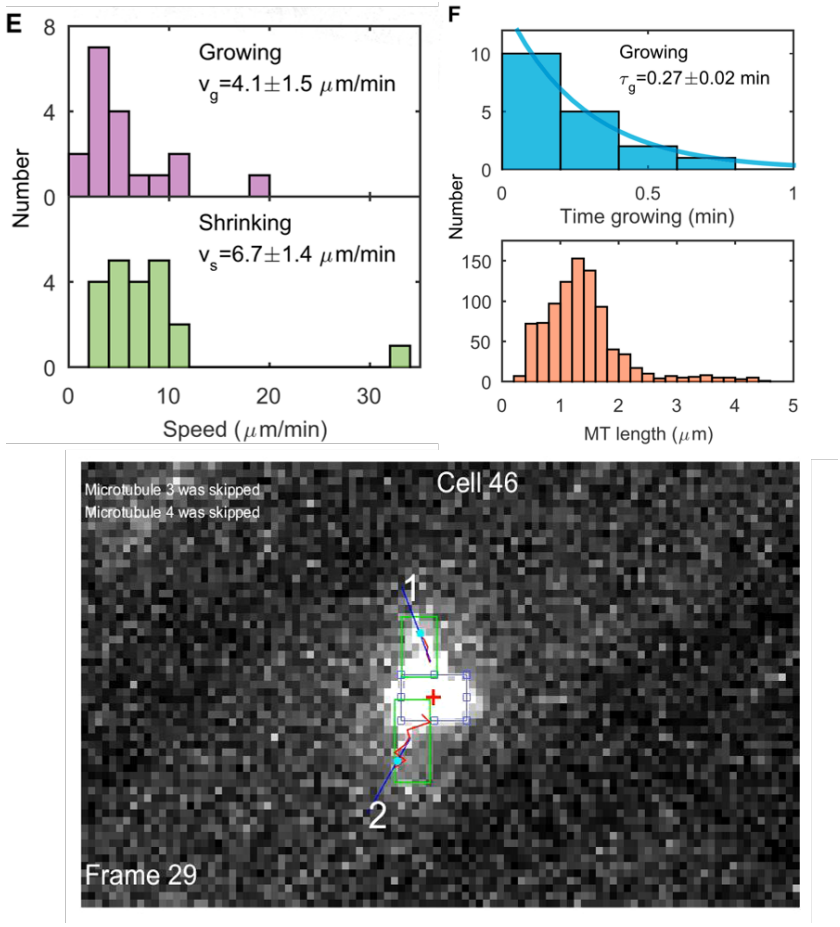

Figure 2.6: This figure demonstrates the results of the TipTracker algorithm in measuring mitotic MTs in fission yeast. It shows data from measuring 20 different MTs in 15 different cells. The upper left histogram shows the spread of growing velocities observed with the median velocity equal to 4.1 $\frac{\mu m}{s}$. The upper right histogram shows the distribution of growing lifetimes, measured as the time a MT is in a growing state before exhibiting a catastrophe. We fit this distribution with an exponential and found a characteristic lifetime of growth as 0.27 minutes. By inverting this lifetime, we can determine a frequency of catastrophe which we found to be 3.7 min^{-1}. The lower left histogram shows the measured shrinking velocities, with he median speed being 6.7 $\frac{\mu m}{s}$. The lower right histogram depicts the measured lengths of MTs, with an average length of 1.31 μm. We only recorded one rescue event which provided an upper bound on their frequency to be roughly 0.175 min^{-1}. The lower image shows a sample result of the TipTracker analyzed data.

However, the algorithm underlying TipTracker has inherent limitations that make it unsuit-

able for further usage in this project to quantify the dynamics of mitotic MTs. The dominant drawback inherent to the algorithm is its reliance on the user inputs to find the MT and to locate its tip. This semi-automatic aspect of the program means that the user is required to input 2 clicks per MT per frame. So, for a typical monopolar spindle that has 5 arms and is imaged for 120 frames, this would mean 1,200 clicks required by the user to quantify the dynamics of only 5 MTs. Unfortunately, due to the heterogeneity in the MT population, large numbers of arms are needed to be sampled to extract subtle trends and more accurate parameter values. Generating a large amount of analyzed data is not practical with the TipTracker algorithm because of the reliance on the user. A new fully-automated algorithm that detects MTs and measures them throughout the image series is necessary for continuing this research.

2.4.1.2 Generative Model Fitting

Due to the large volume of microscopy data generated and the heterogeneity of individual MTs, it is essential to establish an accurate, fully automated, method to measure the lengths of MTs throughout a series of frames. The low signal to noise ratio of the MTs makes automated detection difficult and the dynamic nature of MTs makes the tracking difficult. I implemented a routine that detects features by using a generative model framework that determines the statistically relevant features in the image and fits predetermined mathematical functions to their intensity profile. I then pass these detected features to a tracking routine that is based on a linear assignment problem that connects the identified objects between frames to produce the lowest cost collection of tracks. Generative model fitting allows for fully automated detection and tracking of MTs throughout image series.

Detecting Features

Generative model fitting is based on the simple idea that if we can produce an exact replica of the image of interest, then we know exactly which objects are present and where they are located [73, 77, 78]. We use an iterative process to generate a model image and fit that to the real image such that their discrepancy is minimized. I will describe each step of the algorithm and the preliminary

results from this improved method.

•Identify Mitotic Cell

The task of discerning which cells are mitotic from a field of view of cells is difficult to fully automate. A sample field of view of cells is shown in figure 2.7 and the mitotic cells appear to have a bright object in their center. This bright feature is how the monopolar spindle appears on the camera and is the distinguishing characteristic of a mitotic cell. I implemented a combination of Gaussian smoothing, morphological image processing, and an intensity threshold to produce a mask that distinguishes mitotic cells (shown in figure 2.7. With the locations of mitotic cells known and a mask created, I now cropped individual image series for each cell of interest that will be fed to the analysis program. Proper cropping of the images is an important step because the speed of the analysis program depends on the number of pixels present in the image. By reducing the number of pixels that the generative model must fit to, we rapidly speed up the analysis with tightly cropped images.

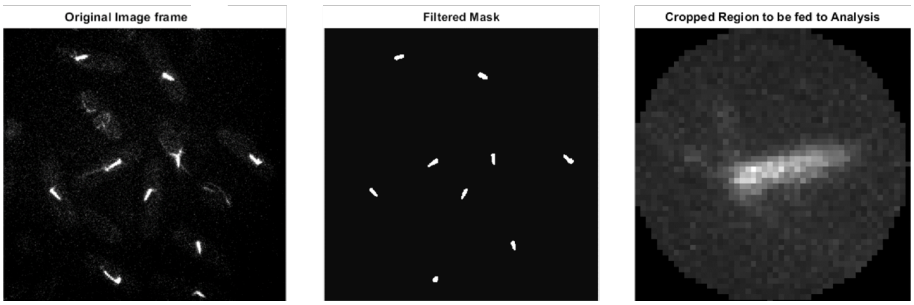

Figure 2.7: These frames illustrate the successful automatic cropping of monopolar spindles. The left most frame shows a field of view of cells, with and without spindles. The middle frame shows a threshold mask based on intensity after morphological image processing. The last frame on the right shows a sample of a cropped spindle that will be directly fed into the analysis program. It is important to properly crop the spindles because analysis speed depends on the number of pixels present in the image.

•Generating a Model Image

The cropped images of monopolar spindles are now fed into the feature detection portion of the code that attempts to generate a model image that minimizes the discrepancy with the actual data. My

method closely resembles that of the Jaqaman lab who used this type of algorithm to track point particles in micrographs [77, 78] The first step is to provide an initial guess of how many features may be present and the shape of their intensity profiles. For MTs nucleating from a monopolar spindle, I set this initial guess to four MTs present and their expected intensity profile should be a line Gaussians because they are polymerized of tubulin dimers that individually produce a point Gaussian and polymerize into the profile of a line Gaussian. I also specify that one point Gaussian should be present because of the intensity profile of the two colocalized SPBs. With the initial number of features to fit and their expected shapes specified, I now allow the algorithm to guess on position and placement in order to produce a simulated image. In order to optimize the speed of the algorithm, I program it to run on parallel processors and use eight different initial guesses. Each initial guess improves based on a gradient descent method that gradually converges to a local minimum in the hyper-dimensional parameter space of this image fitting process. Once all of the initial guesses have converged to local minimum, I select the lowest of these minima and use it as the generative model image. A representative generated image is shown in figure 2.8.

With the initial generative model image created, I now determine the residual value. This residual value is the sum of squared intensity differences between the generated image and real image at every pixel. A perfect generated image has a residual value of zero. However, as seen in the example fit in figure 2.8, the residuals are never perfect due to an inability of any model to completely describe the biological data. With the residual value calculated, the algorithm now reiterates the entire image generating process with one additional MT allowed. This means that the algorithm now uses 5 MTs in its image generation and then quantifies how well this does based on the residual value. In order to properly quantify whether the additional feature is warranted and not just an artificial improvement in the residual value because of over fitting, the algorithm implements an F-test to quantify whether adding the feature is statistically significant relative to the change in residual value. After adding the maximum number of significant features, the algorithm then attempts to remove features to see if that leads to a better residual value. Similar to the feature addition procedure, the removal of features continues until the change in residual

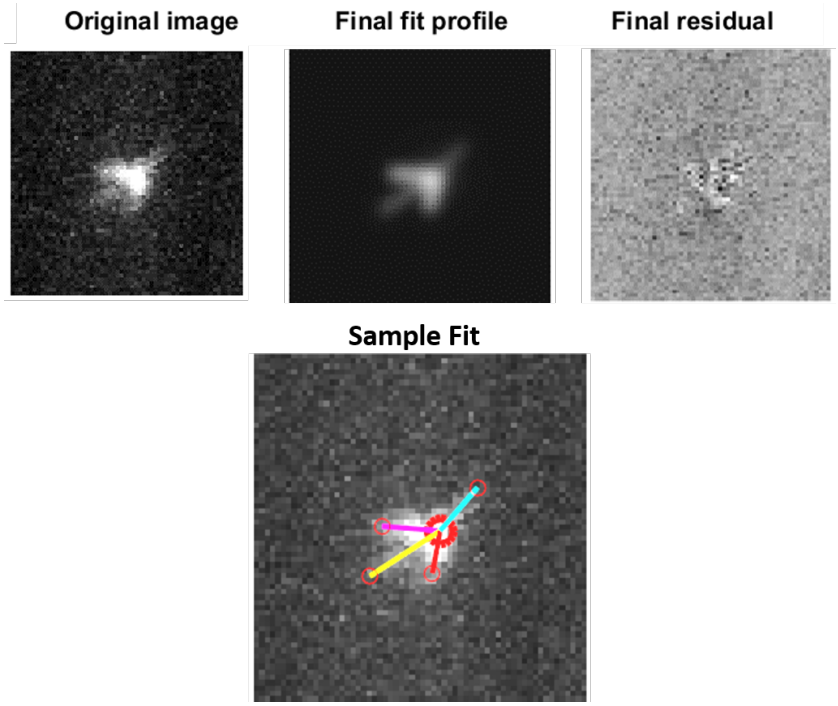

Figure 2.8: These frames show the successful feature detection of a monopolar spindle. This automated image analysis method begins by taking in the cropped image, shown in the upper left. The algorithm then attempts to generate its own image based on predefined intensity profiles. The quality of this generated image is measured by summing the squared differences at each pixel between the original image and the generated image. When the residual obtains a minimum, the fit routine is complete. The generated image is shown in the center of the top row, and an example residual is on the upper right. Finally, with the image generated, we have essentially fit the data. This fit result is shown in the bottom image.

relative to the number of features is no longer acceptable, based on the F-test. This iterative process of generating images, calculating residual, and adding or removing features results in a novel image detection algorithm that detects MTs in mitotic cells. An example of what the fit result looks like is shown in figure 2.8. The annotated fit image displays the approximated MTs with colored lines and the location of the SPBs with a red circle. The estimated length of the MTs will be between the center of the fit Gaussian (red circle) and tip of the MT (end of the colored line).

Tracking Features

Upon determining the presence and location of relevant features in the micrograph, it is necessary to connect these features throughout multiple images as to be able to analyze their dynamics over time. Tracking features is a type of feature detection that occurs with the extra dimension of time. This added dimension greatly increases the difficulty of the problem and requires significant amount of work to allow the computer to automatically connect features throughout images [77, 79]. We employed the theoretical framework known as the linear assignment problem (LAP) to track MTs throughout images. The LAP is essentially a minimization problem that tries to reduce the costs of connecting features with each other in consecutive frames. Tracking features with the LAP allowed us to generate movie length tracks of MTs in a fully automated manner.

The LAP is based upon the notion of minimizing costs that are predefined by the user. A simple example of a cost is absolute distance separating two objects. If we imagine two MTs near each other in two consecutive frames. How would we assign the MTs labels in each of the frame? A basic cost we could implement to determine this linkage would be to calculate the distance of the MT tips from each other in the consecutive frames.

$$c_{i,i+1} = \delta_{i,i+1} = \sqrt{(x_i - x_{i+1})^2 + (y_i - y_{i+1})^2}$$

Where the tip coordinates of an MT at frame i are $[x_i, y_i]$ and of a

proposed connecting MT tip at frame i+1 are $[x_{i+1}, y_{i+1}]$.

We can then sum up the distances between MTs in consecutive frames and this summation is the

value we want to minimize. Using this cost will result in the connection of MTs that are spatially close to each other.

However, we can improve upon our frame to frame linking by altering the cost definition. An exampleof this is not minimizing the absolute separation of features, δ, but give different weights to different components of the distance. Specifically, we know from a physiological basis that MTs are much more likely to grow and shrink along a linear axis than they are to pivot. To improve our tracking performance, we can modify our cost to give preference to MTs that are closer in radial distance than angular distance. We can rewrite the distance in polar coordinates and then apply a weighting parameter that leads to better tracking. This modified cost takes the form:

$$c_{i,i+1} = \delta_{i,i+1} = \sqrt{r_i^2 + r_{i+1}^2 - 2r_i r_{i+1}\cos\left(\theta_i - \theta_{i+1}\right)}$$

Where the tip coordinates of an MT at frame i are $[r_i, \theta_i]$ and of a proposed connecting MT tip at frame i+1 are $[r_{i+1}, \theta_{i+1}]$.

In general, there are multiple objects we are connecting and multiple potential costs we can associate with each object in a given frame. For the specific case of tracking MTs, these objects can grow, shrink, merge, or split between any two frames. It is easy to see how rapidly the complexity of this sort of algorithm grows. If we consider a typical monopolar spindle with 5 arms in each frame and attempt to connect the features between consecutive frames, there are 4^5 possible cost assignments. However, we can rule out a large number of these possible assignments by imposing threshold values that immediately discard cost assignments. The implementation of threshold values combined with clever cost definitions allowed us to accurately connect features between consecutive frames.

With linkages between frames established based on minimizing costs, we can now link these consecutive frame linkages throughout the entire image series. The linkage of linkages is a recursive operation that resembles a dynamic programming routine. We initially associated MTs in consecutive frames based on minimizing cost and now we can associate MTs present in pairs of consecutive frames with each other in order to minimize the costs. This routine can be followed through and

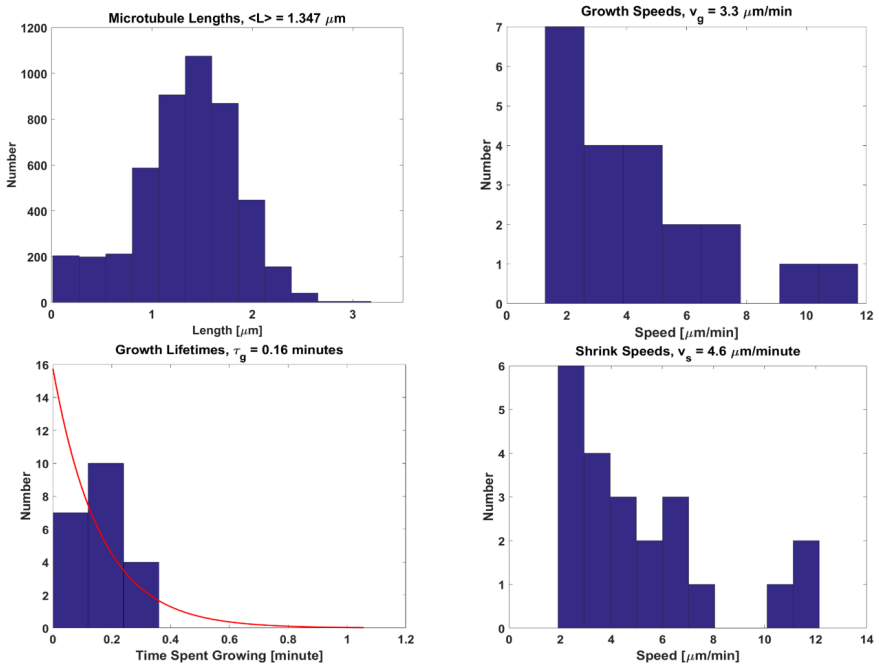

Figure 2.9: The histograms represent data measured by the automated analysis routine on 8 different wild type yeast cells. The MT length histogram is in the top left and reports and average length of 1.347 μm. The top right depicts the spread of growth speeds recorded with the median growth speed being 3.3 $\frac{\mu m}{s}$. The lower left depicts the spread of growth lifetimes, the time in a growing state before catastrophe. We can fit an exponential to this distribution and determine a characteristic lifetime of 0.16 minutes. By inverting the lifetime, we see that this produces a catastrophe frequency of 6.3 min^{-1}. Lastly, on the lower right, we have the spread of shrinkage speeds with the median speed being 4.6 $\frac{\mu m}{s}$. It is not shown, but there were 6 possible rescue events seen in the collection of data. By fitting an exponential to this distribution, we can bound the rescue frequency by $\leq 2.86\ min^{-1}$.

result in full movie length tracks of MTs that are the most likely based on our costs. Figure 2.9 shows preliminary results from this tracking code as well as a series of still shots that represent the tracking combined with the generative model feature detection.

This image analysis work has resulted in a better range on possible dynamic instability parameters. The next step will be to expand to 3D (discussed in chapter 3) and to generate larger numbers of measurements. As a summary, figure 2.10 are the two different sets of parameters produced by TipTracker and the automated generative model algorithm

2.5 Bleaching Experiments

To complement the significant amount of effort put towards the quantification of MTs in monopolar spindles, we performed bleaching experiments in both monopolar and early bipolar spindles in order to quantify the differences in dynamics of MTs in these different mitotic states. The overall goal of this research is to understand the relationship between MTs, spindle, and chromosomes during mitosis. In order to address this question, it is essential to determine whether there are distinct dynamic phases of MTs that correspond with stages of mitosis. Specifically, how do the different conformations of MTs during mitosis change their dynamics and how are these altered dynamics utilized by the cell for chromosome segregation? To address this vein of research, it is necessary to implement experimental methods beyond direct imaging with feature detection and tracking.

Fluorescence recovery after photobleaching (FRAP) is a technique I used to quantify the difference in MT dynamics between a monopolar and bipolar spindle state. We implemented this method because it is impossible to resolve MTs when they are interdigitated in the early spindle due to the diffraction limit of light. Because these spindle MTs are not resolvable in micrographs, we cannot apply the image analysis software to quantify the MT dynamics. To circumvent this obstacle, we utilized photobleaching and the corresponding intensity recovery to get an idea of the chemical kinetics of the tubulin subunits comprising the MTs. The technique of bleaching mitotic spindles to garner information about the underlying MT dynamics was used by Maddox *etal*. where

Generative Model Results

$$\mathbf{v_s} = 4.6\ \frac{\mu\mathbf{m}}{\mathbf{min}}$$

$$\mathbf{v_g} = 3.3\ \frac{\mu\mathbf{m}}{\mathbf{min}}$$

$$\mathbf{f_c} = 6.3\,\mathbf{min^{-1}}$$

$$\mathbf{f_r} \leq 2.86\,\mathbf{min^{-1}}$$

$$< \mathbf{L} >= 1.35 \pm 0.05\,\mu\mathbf{m}$$

TipTracker Results

$$\mathbf{v_s} = 6.7\ \frac{\mu\mathbf{m}}{\mathbf{min}}$$

$$\mathbf{v_g} = 4.1\ \frac{\mu\mathbf{m}}{\mathbf{min}}$$

$$\mathbf{f_c} = 3.7\,\mathbf{min^{-1}}$$

$$\mathbf{f_r} \leq 0.175\,\mathbf{min^{-1}}$$

$$< \mathbf{L} >= 1.31 \pm 0.02\,\mu\mathbf{m}$$

Figure 2.10: This figure shows a comparison of the dynamic instability parameters and average MT length recorded by each analysis software. The values are in good agreement with each other. The significant different in rescue frequency should not be overly interpreted because of the very small number of events recorded (1 for TipTracker and 6 for the Generative Model Method). The very close similarity in average lengths indicated that each analysis software is identifying the same group of MTs, possibly indicating the same implicit bias for longer MTs over shorter MTs.

they bleached MTs in budding yeast during interphase and mitosis and determined difference in MT dynamics between these two cell cycle stages [57]. I utilized their published results as an outline for how to analyze the intensity recovery and connect it to MT dynamics. However, rather than focus on mitosis vs. interphase MTs, I narrowed the analysis to differences in MT dynamics within mitosis itself. This work represents the first FRAP experiments performed in fission yeast and resulted in half life values for the tubulin subunits in monopolar spindles and early metaphase spindles. I hope this research will provide a foundation for performing more detailed and innovative bleaching experiments in fission yeast, which I discuss in chapter 3.

In our own work, we attempted to fit a function derived from a first order rate law in order to determine the half life of the polymerized tubulin in the MTs. The assumption that the tubulin exchange in an MT is first order makes intuitive sense because the polymerization rates of MTs should scale linearly with the tubulin concentration present because there is no intermediary rate limiting steps in this reaction pathway. The derivation of our fitting function centers around the intensity at bleaching, I(t = 0), the maximum recovery value, I(t = t_f), and a basic rate equation with the slight modification that the typical concentration is replaced with the difference between maximum intensity and intensity at time t. The replacement of concentration with intensity difference is based on the direct relationship between the number of unbleached molecules and the intensity difference. This is shown as:

Define: A(t) = I(t = t_f) - I(t)

Then: $\frac{dA(t)}{dt}$ = -kA(t) (rate law)

We can solve this differential equation, which results in:

$$\int_0^t \frac{1}{A(t)} dA(t) = \int_0^t -k dt$$

$$\ln A(t) - \ln A(t=0) = -kt$$

$$A(t) = A(t=0)e^{-kt}$$

So, we can now plug in the intensity values:

$$[I(t=t_f) - I(t)] = [I(t=t_f) - I(t=0)]e^{-kt} \tag{2.1}$$

This derivation shows the theory behind our FRAP experiments. In equation 2.1, it is common to set $k = t_{1/2}$ and this is the value we are attempting to solve evaluate because it describes the turnover rate of the tubulin dimers in the spindle. In order to produce recovery curves that can be analyzed, I wrote software that allows the user to draw a 6x6 pixel box around the bleached area and record the intensity in this region throughout the image series. These measurements produced a raw intensity recovery curve that needed to be corrected for background level and photobleaching due to imaging (not the intended bleaching from the experiment). I adjusted for the background signal by subtracting off the background level which I determined by averaging over four different background regions in the image. I corrected for image bleaching by monitoring the intensity level of a control cell over time and recording how much it decreased throughout the movie. I then fit a linear line to the control cell's intensity profile and used the slope of this line as the bleaching rate. With the bleaching rate approximated, I am able to correct the cell of interests intensity level to account for it. I performed this experimental protocol and analysis on both monopolar and early bipolar spindles which resulted in the recovery profiles and theoretical fits shown in 2.11.

The results of the FRAP experiments are half life times that describe the rates of tubulin turnover in the spindle. The procedure allows us to quantify the dynamics of MTs that are irresolvable because they are bundled in the spindle. From the fits to the measured recovery curves, we see that the bipolar spindle has a half life of roughly 43 seconds whereas the monopolar spindle has a half life of 75 seconds. This significant difference in recovery speed implies that the kinetics of the tubulin heterodimers in the spindle are much quicker for the early metaphase spindle than for the monopolar state. Quantifying the half life times is an important step, but it is insufficient to directly approximate the dynamic instability parameters. The process required to connect the half life time to actual dynamics parameters will require thought of an appropriate model to make this connection. Also, we may be able to connect the half life in recovery time to dynamics by constructing a simulation that takes dynamic parameters as inputs, and then we can measure a simulated recovery time. Ideally, if we have inputted the appropriate dynamic parameters, then we will reproduce the appropriate half life time. Although there is more work to be done to make the

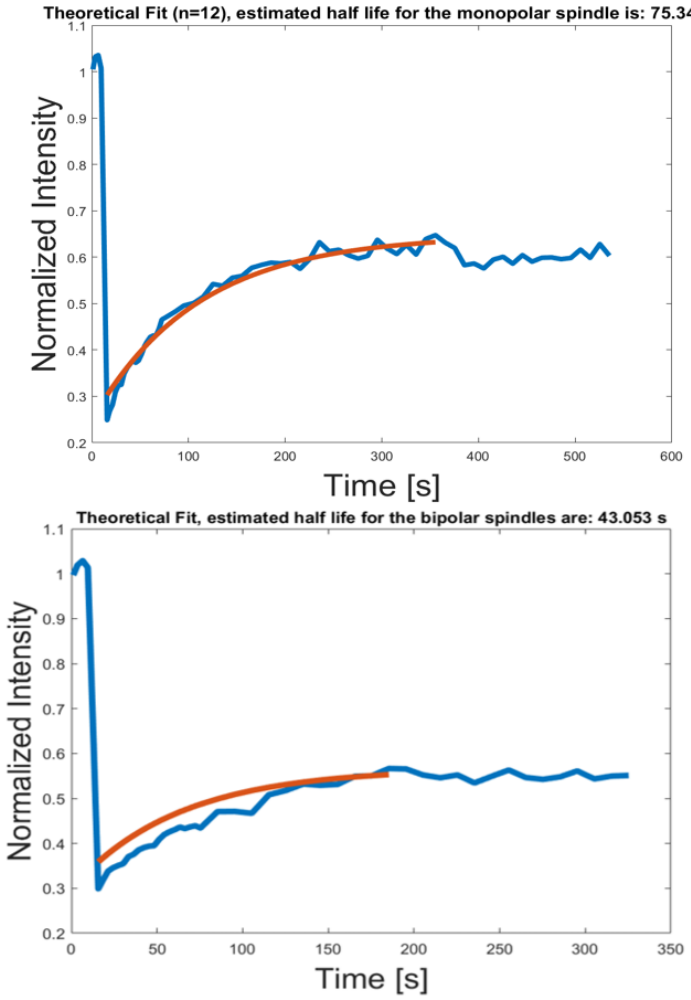

Figure 2.11: This figure shows two different FRAP curves, one from the monopolar state (top) and one from the early bipolar state (bottom). The recovery half life for the monopolar state is 75.342 seconds and for the bipolar spindle is 43.053 seconds. The difference in the recovery times suggest that tubulin heterodimers are turned over at a faster rate in the early bipolar spindle than in the monopolar spindle. Curves used in the fitting are shown in equation 2.1.

FRAP recovery data useful,this work marks the first bleaching experiments performed on fission yeast spindles.

2.6 Modeling the Monopolar Spindle

While the combination of microscopy and image analysis has produced preliminary MT dynamics quantification, it is not enough on its own to depict the reliance of the spindle on MT dynamics. Mathematical models of the bipolar spindle formation and function have been an area of active research for decades and remains filled with unanswered questions [3, 16, 36]. I have created a novel kinetic Monte Carlo model of the monopolar spindle state as a means to connect the observed dynamics to the overall spindle behavior. I have also utilized this model as a means to generate simulated data that can be used to benchmark the previously described image analysis software. The combination of experimental techniques with computational models represents a new strain of biological research that will allow for scientists to pursue biological questions from unexplored viewpoints.

Kinetic Monte Carlo models are a probabilistic model that defines the evolution of a system through time. In order for a system to be appropriately described by a kinetic Monte Carlo model, it must exhibit defined rates of transition between different states. The first implementation of a kinetic Monte Carlo model came from Young and Elcock in 1966 and was soon followed by the work of Dan Gillespsie who applied this probabilistic model to chemical reactions and developed the Gillepsie algorithm for implementing kinetic Monte Carlo models [16, 80]. This development of applying stochastic models to biological systems has grown since then and is now a common technique in formulating a mathematical framework for addressing biological research questions. Specific to this work, I applied a kinetic Monte Carlo model that described the polymerization patterns of mitotic MTs by simulating stochastic transitions between states of growth and shrinkage [43]. The general scheme behind the MT kinetic Monte Carlo description is shown in fig. 2.12. By applying this dynamical model to each individual MT, and modeling multiple MTs nucleating from a single pole, I have developed a primitive simulation technique to model the monopolar spindles

studied in this project.

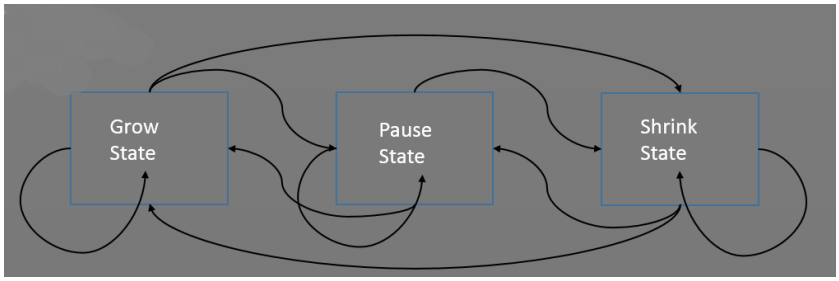

Figure 2.12: This diagram shows the underlying state transitions of a microtubule. The MT has been seen to exist in three states; growth, shrinkage, or pause. The transitions between growth and shrinkage states are named catastrophe (for growth to shrinkage) and rescues (for shrinkage to growth). Once in a given state, there is the associated probability to either grow/shrink or transition to a different polymerization state. The existence of a pause state only applies to bundled MTs and is not totally understood but has been observed.

The goal of my kinetic Monte Carlo monopolar spindle model is to tune the dynamic parameters of the model in order to reproduce the observed behavior measured in our microscopy data, both from the direct image analysis as well as in the bleach recovery experiments. I aimed at using a minimal parameter model as to not over fit the data and artificially match the observed behavior. The model was 2 dimensional in space and consisted of a given number of MTs nucleating from a single point in space at a random orientation. The MTs are randomly assigned as either singles or bundles where each classification exhibits separate dynamics. The main difference in dynamics between the two types of MTs is that only bundles exhibit a pause state. The parameters values for the MTs implemented come from previous work and are specified in the labs previous publication describing a kinetic Monte Carlo spindle formation model that includes proteins and Brownian motion, see fig 2.13 for the relevant parameter values [16]. We can convert these parameter values into probabilities by multiplying them by a small enough time step such that we only expect at most one event to occur per time step. Once in a state, the MT has a chance to change length or to transition to a different state. Due to simplicity, the MTs can only grow or shrink by the length of a tubulin dimer per time step. The model took the computational form of iterating over time steps where within each time step the individual MTs have the ability to switch states and change

lengths. An important requirement of the simulation is that the time step must be sufficiently small as to ensure that specific transition probabilities are well below one as to ensure capturing the stochastic nature of the system.

Slow dynamic instability model				
Growth speed	v_g	2.7 μm min^{-1}	0.7–11 μm min^{-1}	Kalinina et al. (24)
Shrinking speed	v_s	3.8 μm min^{-1}	1–16 μm min^{-1}	Kalinina et al. (24)
Grow-to-pause frequency	f_{+0}	1.8 min^{-1}	0.4–7.1 min^{-1}	Kalinina et al. (24)
Shrink-to-pause frequency	f_{-0}	2.53 min^{-1}	1.2–5 min^{-1}	Kalinina et al. (24)
Pause-to-shrink frequency	f_{0-}	0.49 min^{-1}	0.2–1 min^{-1}	Kalinina et al. (24)
Pause-to-grow frequency	f_{0+}	0 min^{-1}	—	Transitions from pausing to growing appeared infrequent in Kalinina et al. (24)
Fast dynamic instability model				
Growth speed	v_g	4.1 μm min^{-1}	1–10 μm min^{-1}	This work
Shrinking speed	v_s	6.7 μm min^{-1}	5–25 μm min^{-1}	This work and Sagolla et al. [32]
Catastrophe frequency	f_{cat}	3.7 min^{-1}	1–8 min^{-1}	This work
Rescue frequency	f_{res}	0.175 min^{-1}	0–8 min^{-1}	This work

Figure 2.13: These parameter values come from our previous publication [16] and describe the relevant values used in a monopolar spindle simulation. For the simple spindle model that I used, I implemented the conversion frequencies between states as well as the growth and shrink velocities. The goal of the image analysis portion, previously described, will be to further improve upon these parameter value estimations which were mostly found with the TipTracker method.

2.6.1 Benchmarking Analysis Software with Simulation

The development of image analysis software is not complete until the limitations of the algorithm are tested and quantified. For the purposes of measuring the performance of the feature detection and tracking portion of the software, we will determine the percentage of MTs that were properly recognized and followed throughout an image series. We will also take note of how often there is a false identification or a missed identification. Because we do not know where the MTs are in the experimental images, we need to generate simulated images where the objects' locations are exactly known and then feed them to the image analysis software to quantify its performance. The process of measuring performance by running the software on simulated data that has exact features known is called benchmarking and is necessary to gauge how reliable the software is. I benchmarked the previously described image analysis software by creating simulated images with the above kinetic Monte Carlo monopolar spindle model. I visualized the dynamics generated by the algorithm and then visualized them in a movie using MATLAB. I then applied background noise

and a Gaussian intensity profile to the MTs in order to mimic the observed image data captured on the microscope. This resulted in simulated image data, shown in figure 2.14, that I plan to use in order to determine how well our analysis software performs.

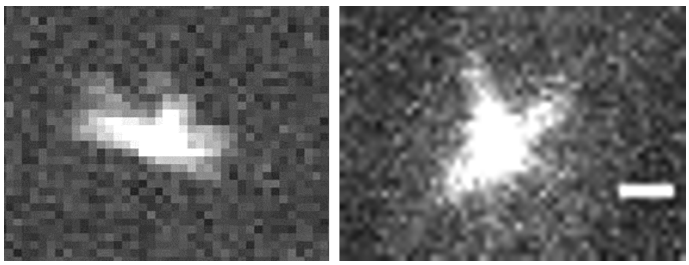

Figure 2.14: This depicts a comparison between real and simulated image data. The simulated data is on the left and the real data is on the right (where the scale bar indicates 1 micron). The benefit of being able to generate simulated data is that it can be used to benchmark the performance of our image analysis software. Simulated data allows for control of various parameters, such as background level and number of arms present. This effort will give us an idea of which regimes our analysis software struggles.

I also used the kinetic Monte Carlo simulation to model our FRAP experiments in monopolar spindles. I modeled the bleaching laser as a Gaussian profile where the tubulin dimers have a probability of bleaching based on their position relative to the center of the bleaching laser. This effectively allowed form the simulation of the bleaching experiments as well as the replacement of bleached tubulin with unbleached tubulin. I ran the simulations with the same number of arms (6 singles and 3 bundles) and the same dynamic parameters. In order to reduce noise, I averaged 5 different recovery curves. The result is shown below:

It is important to note the discrepancy between the simulated half life time and the half life times measured for both monopolar and bipolar spindles in the experimental data. My simulation produces a recovery that is much quicker than either, and especially quicker than the experimental monopolar spindle (75 seconds compared to 34 seconds). There are many possible explanations for this difference: number of arms, modeling of the bleaching laser, the size of the tubulin pool, and the dynamic parameters. It will be essential to figure out which subset of these possible explanations are causing the accelerated recovery time in the simulated spindles.

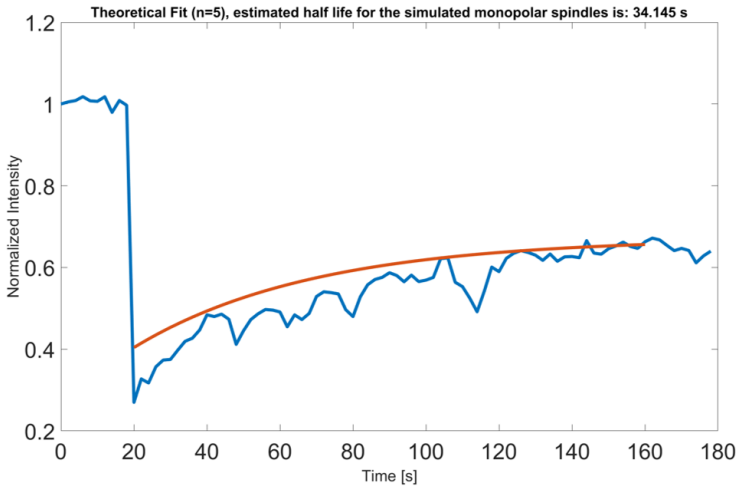

Figure 2.15: This is an intensity recovery curve after bleaching the simulated monopolar spindles. I used monopolar spindle simulations with 3 bundles and 6 single MTs. I modeled the bleaching laser as a Gaussian profile where the tubulin dimers had a probability to be bleached based on their proximity to the bleaching laser. I fit the same expected recovery curve to the raw measurements and determined a half life time of roughly 34 seconds. This is noticeably faster than the experimentally measured recovery curve of the monopolar spindle, suggesting a shortcoming of the simulation.

Chapter 3

Discussion on Past and Future Work

3.1 Reflection on the Progress Made

The goal of this research is to better quantify the dynamics of mitotic MTs *in vio* in order to improve parameter values essential for accurate simulations of spindle formation [16]. Mitosis has a long history of study, yet still remains enigmatic. Traditional biological methods were able to identify the stages of mitosis, regulatory pathways that govern these stages, and the key molecular players involved in these stages. With this groundwork laid, it is now time to ask system level questions of how these individual molecular players interact to form macro molecular complexes that faithfully perform the absolutely critical task of equal division of chromosomes during division. New questions and answers will follow from a new perspective that aims to determine the synergy and cooperation essential for proper spindle formation and a successful mitosis. Improved technologies will allow for researchers to manipulate and interrogate the dividing cell in unprecedented ways to garner knowledge about the physical characteristics of the interactions during chromosome segregation. The unifying goal of this diverse range of research will be to provide conclusive explanations of why mitosis fails and how this knowledge may be utilized to develop pharmaceuticals targeted at cells with aberrant cell cycles.

I have assisted in this study of mitosis by helping to develop a library of fission yeast strains, a microscopy protocol, and computational tools to quantify the dynamics of MTs. Specifically, I have helped create forty different strains of fission yeast with various mutations that allow for a prolonged looked at fluorescently labeled MTs in a cell stalled at early mitosis, developed an imaging procedure

to capture the dynamics of MTs with high spatiotemporal resolution, and authored image analysis software to extract biological meaning from the micrographs. To complement the image analysis effort, I have authored a minimal parameter model to produce simulated images that can be used to quantify the software's performance. Lastly, I have utilized bleaching experiments in order to better quantify the dynamics of unresolvable mitotic MTs interdigitated in an early metaphase spindle and written software to automate the analysis of this data. Taken as a whole, this work has led to the development of both experimental and computational techniques that will allow us to better understand the behavior of MTs in early mitosis, a critical step toward better understanding the physical basis of cell division.

3.2 Ideas for Future Work

Although some progress has been made, there are still plenty of unexplored areas of research to pursue. Many of these research areas build upon methods that I have preliminary developed, such as image analysis and mutant yeast strains. By further pursuing these avenues of inquiry, it may be possible to further discern MT dynamics as well as to begin the quantification of other essential simulation parameters. Also, continued effort to better understand how to extract meaning from micrographs is an area of research that applies to nearly all biological research. The ability to garner biological insight from still images or series of images is crucial in this current age of advanced microscopy. While technological progression is allowing for better resolution on the microscope, there needs to be corresponding progress made in our ability to interpret what we see on these micrographs. In pursuing this future work, I think it is essential to keep in mind the broader applications of quantifying physical parameters from noisy images. The future of biological research depends on our ability to visualize, manipulate, and understand the model organisms we study, and image analysis will play a role in this effort.

The rest of this chapter focuses on specific topics that will complement or expand upon the progress I have made in this research. These topics are not equal in scope or effort required to complete them, but are areas that I would pursue if I were to continue working on this project and

the effort to better quantify physical parameters and molecular players in early mitosis.

3.2.1 Cross Strain Comparison

An obvious next step in this research is to utilize the strain library to quantify the effect of microtubule associated proteins (MAPs) on MT dynamics and spindle formation. Our experimental work has resulted in a collection of fission yeast strains with the MTs fluorescently labeled and the cut7-ts allele present to inhibit mitosis. In combination with these foundational mutations, we have added fluorescent labels on other cellular structures and deleted various MAPs. To generate a clearer picture of the mitotic physical system, we have began to explore using various fluorescent membrane proteins to get a sense of membrane deformation and MT membrane interactions. An example of this data is shown in figure 3.1 where the membrane is labeled with a green fluorescent tag. We have also developed strains with the kinetochores labeled as a means to track the location of the chromosomes. The proteins we chose to delete all have known functions in regulating the dynamics of MTs and the result for their deletion on a monopolar spindle is shown in figure 2.4. We hope to better quantify exactly how they alter these dynamics and how this altered dynamic state leads to problems during chromosome segregation. The combination of these strains will allow us to produce images containing different cellular detail that we can attempt to analyze for relevant data quantifying mitosis and what determines its success or failure.

The combination of the biological work to develop a strain library and imaging protocol with the computational tools to analyze the micrographs for physical parameter values will allow for deeper biological insight into mitosis. Our experimental setup allows us to control the occurrence of the mitotic phases and image the exact phenotypic effects these genotype differences cause. We will be able to use all of the software described in this thesis to quantify how exactly the MT dynamics change between these strains. With the quantification complete on multiple strains, we can begin to investigate the biological implications of these results and how they may further our knowledge of mitosis. The ability to image the spatial organization of MAPs, MT dynamics, and spindle formation will lead to a systems level interrogation of mitosis.

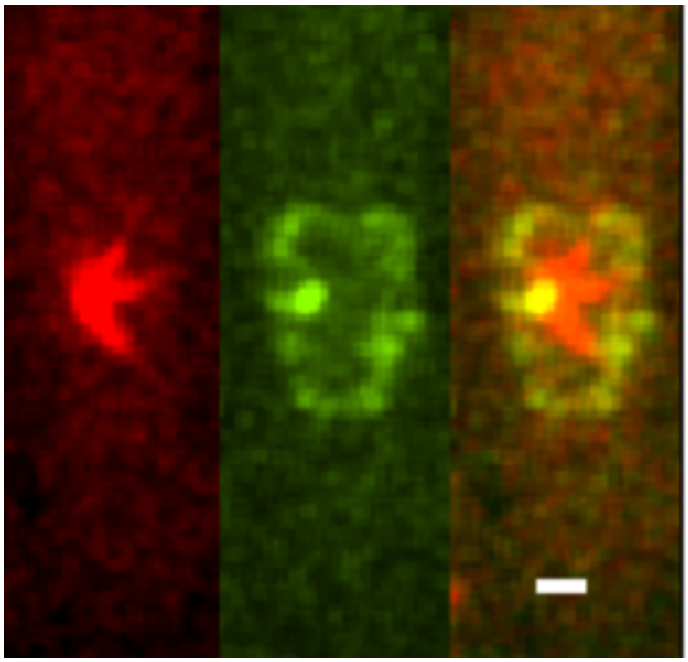

Figure 3.1: This image shows our basis yeast strain combined with a membrane label. We used a cut11-GFP label that tags the nuclear membrane as well as the spindle pole bodies in early mitosis (shown in green). We combined this label with our red MTs and this will allow us to produce a fuller picture of what is happening within the cell during mitosis. Studying how membrane dynamics change in different cells, and how the membranes rigidity may affect the MT dynamics. Labeling the boundary of our monopolar spindle system will help us create more accurate models. (Scale bar represents 1 micron).

3.2.2 3D Kinetic Monte Carlo Simulation

Another immediate next step following this research will be to include another spatial dimension in my current kinetic Monte Carlo monopolar spindle simulation. The need to move the model into three dimensions coincides with the conversion of our image analysis software into three dimensions. Because we are unsure of how significant the compression of the data into two dimensions is on the recorded lengths and dynamics, we hope to start using the data gathered in the third dimension. With a 3D simulation, I will be able to perform many of the similar methods described to benchmark the new 3D image analysis software. The modification to the simulation software will involve altering the intensity profiles applied to the MTs to account for a spread in the z direction. It is important to note that the intensity profile used will be an anisotropic Gaussian profile because microscopes do not resolve objects as well in the axial direction as in the lateral directions. With this applied, I will sample the intensity profiles generated at discrete heights in order to replicate the collection of image stacks. This move to 3D in both analysis and simulation is a natural progression and will produce more accurate results because of the inclusion of more data.

3.2.3 Hidden Markov Model

A hidden Markov model will be implemented to objectively determine whether or not an MT is in a growth, shrinkage, or pause state based on the measured length vs time data produced with the image analysis software. This is an absolutely critical step if we wish to accurately quantify transition frequencies between states because the length vs time data is too noisy to know for sure which state the MT occupies. The noise associated with the dynamics is well represented in sample tracks from the image analysis program, see fig 3.2, and makes it difficult to know exactly whether the MT has a GTP cap or not. Because it is essential to know how often the MTs interconvert between polymerization states, we need a statistically significant test to provide the best possible estimate of MT states based on their length vs time data. I plan to pursue the development of a

hidden Markov model to accomplish this task.

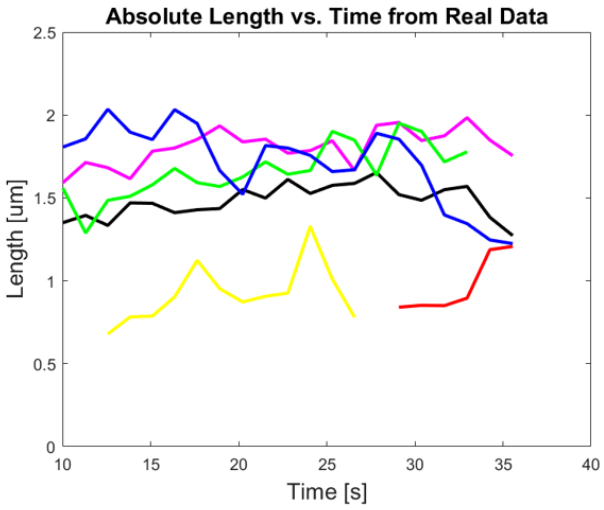

Figure 3.2: This convoluted graph demonstrates the necessity of an hidden Markov Model (HMM) to determine the states of the MTs. The graph is the returned length vs time data from the previously described tracking software. In order to make use of this analysis data, we need to be able to quantify states transitions as well as properly associate polymerization speeds with the state of the MT. An ideal HMM will be able to annotate this length vs time data such that the most probable phase of the MT at a given length measurement is known.

Hidden Markov models (HMMs) describe memoryless systems that switch between unobservable states. A system that is memoryless is called a Markov system and has the property that future behavior only depends on the current state of the system and not on its past behavior. This means that the probability associated with possible state transitions is a function of only the current state of the system, not the large number of possible paths that led to the current state. This property greatly simplifies the mathematics behind such systems because the independence from past behavior significantly reduces the number of relevant variables to take into account. Hidden Markov models predict the most likely sequence of states based on some observable variable. The common terminology used to describe HMMs is that the model generates the most likely sequence of hidden states based on an emission variable. In regards to the MT data, we hope that the model will predict the most likely sequence of hidden polymerization states based on the emitted length data. Ideally, the HMM will be able to accept the length vs time data produced by the

image analysis and annotate it such that the most likely polymerization state is established. With this automated processing of the dynamics data, we will be able to accurately generate parameter values of state transition frequency and polymerization speeds.

3.2.4 Improved FRAP and FRAP Analysis

On of the dominant drawbacks of using a bleaching method such as FRAP is that bleaching a large number of fluorescent molecules inside of the cell causes irreparable damage to the cell. Bleaching damages the cell because it creates a reactive radical or completely denatures the tagged protein. However, we can avoid this damage on the cell by using fluorescent tags that are more likely to change color than to bleach. These photoactivatable fluorescent proteins have the incredible ability that they do not bleach but exhibit a conformational change such that their energy levels shift from allowing one color of emission to a different color of emission. We could photoactivate rather than bleach tubulin dimers and then follow the subpopulation that is now a different color in the microscope. This techniques provides the same abilities as the FRAP used here, but it will damage the cellular structures less and may lead to more repeatable experiments.

Another improvement to the FRAP experiments will be to devise a better analysis method in which to gather more physical information about the MT dynamics. The current technique is limited to analyzing one averaged spot on a 2D image and correcting for background signal. A significant improvement to this method will be the analysis of intensity recovery in 3D on both the monopolar and bipolar spindles. We can alter the image acquisition in order to take image stacks with only 200 nanometer spacing as to provide more data about the intensity profile in the axial dimension. The ultimate goal of this 3D analysis will be to create a simulative model of how the intensity recovers throughout a cross section of the monopolar and bipolar spindles. By analyzing the intensity throughout the depth of the spindle, it may be possible to observe a variation in chemical kinetics as a function of position. This proposed function would be incredibly important to understanding the structure of the mitotic spindle and how to simulate them more accurately.

Lastly, modification to the bipolar FRAP analysis may allow for a better elucidation of how

the chemical kinetics of microtubules change relative to the phase of mitosis. Our experimental setup allows us to have precise control of which mitotic phase the cells are in during the imaging. We could bleach mitotic spindles at different phases of mitosis and then observe how the bleached tubulin dimers redistribute along the length of the spindle. Focusing on the redistribution of bleached tubulin dimers may allow for the recognition of spindle characteristics that are not noticeable from only macro spindle characteristics such as length. Figure 3.3 depicts two distinct intensity recovery profiles along the spindle axis at similar times post bleaching. Each spindle was bleached when they were similar lengths, but because the underlying MTs were at different stages of mitosis the final profiles look very different. The discrepancy in the shape of these curves indicates that the MTs exhibited different chemical kinetics during the phases of mitosis. Further elucidation of these variations in MT dynamics during mitosis will allow for a better physical understanding of the mitotic spindle. Furthermore, any simulation of mitosis will need to account for these distinct difference in physical characteristics as mitosis progresses in order to properly describe it.

3.2.5 User Friendly Software

An overall goal of developing software to analyze micrographs is that other researchers will find it useful. In order for scientists unfamiliar with the research to be able to utilize the software it must be written in a way that is user friendly an easy to understand. My own research described in this thesis depended on software from both the Odde lab and the Jaqaman lab to serve as a foundation on which to expand and further develop utility. I hope to continue this trend of making the image analysis software, both MT measurement and FRAP Analysis, publicly available. Transitioning from personal software to software written to be useful when widely distributed requires modifying some of the code structure and user interactions. I hope to create a intuitive graphical user interface (GUI) that will successfully guide users in their usage of our software. My efforts towards making my software more user friendly may allow a large number of scientists to successfully analyze their microscopy data and broaden the our knowledge of the natural world.

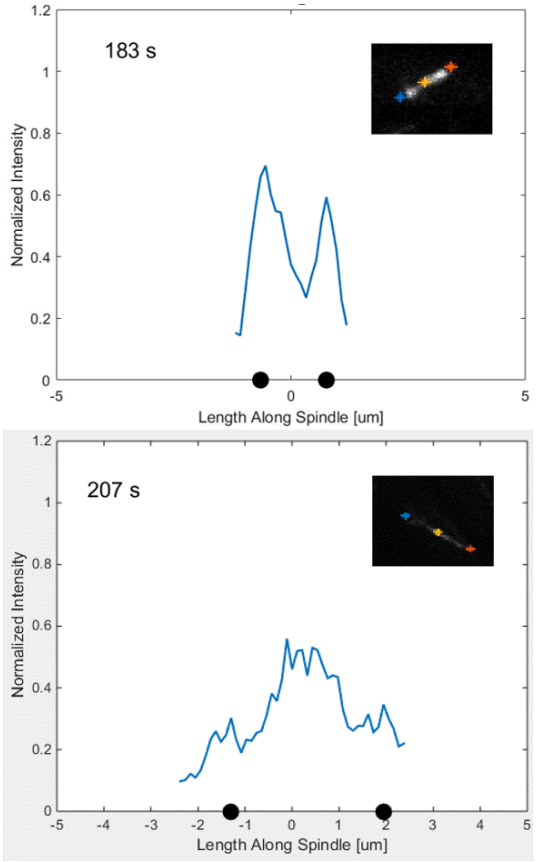

Figure 3.3: This image depicts two very different intensity profiles along the spindle axis in two mitotic cells with similar amounts of time post bleaching. Bleaching was performed on the center of the early bipolar spindle. The top profile shows that after 183 seconds after bleaching the spindle's center, the bleached tubulin subunits are still present and cause the intensity to dip near the middle. The bottom intensity profile depicts a spindle who redistributed the bleached subunits towards the poles, shown by the peak intensity present in the center and the local minimums on each side of this peak intensity region. The estimated position of the SPBs are represented with the black dots on the x-axis and show that the bottom spindle elongated over the time period, implying a different set of kinetics than the top spindle. These differences in redistribution of bleached tubulin dimers may allow for a better quantification of how spindle MT turnover varies in different mitotic phases.

Bibliography

[1] J. Richard McIntosh. Mitosis. Cold Spring Harbor Perspectives in Biology, 8(9):a023218, September 2016.

[2] T. J. Mitchison and E. D. Salmon. Mitosis: a history of division. Nature cell biology, 3(1):E17–E21, 2001.

[3] J. Richard McIntosh, Maxim I. Molodtsov, and Fazly I. Ataullakhanov. Biophysics of mitosis. Quarterly Reviews of Biophysics, 45(02):147–207, May 2012.

[4] Yuta Shimamoto, Yusuke T. Maeda, Shin'ichi Ishiwata, Albert J. Libchaber, and Tarun M. Kapoor. Insights into the Micromechanical Properties of the Metaphase Spindle. Cell, 145(7):1062–1074, June 2011.

[5] Marc Kirschner and Tim Mitchison. Beyond self-assembly: from microtubules to morphogenesis. Cell, 45(3):329–342, 1986.

[6] Hui-Shun Kuan and M D Betterton. Biophysics of filament length regulation by molecular motors. Physical Biology, 10(3):036004, June 2013.

[7] Andrew D. Bicek, Erkan Tzel, Daniel M. Kroll, and David J. Odde. Analysis of Microtubule Curvature. In Methods in Cell Biology, volume 83, pages 237–268. Elsevier, 2007.

[8] Dominique J. Bicout. Greens functions and first passage time distributions for dynamic instability of microtubules. Physical Review E, 56(6):6656, 1997.

[9] S. Dumont and M. Prakash. Emergent mechanics of biological structures. Molecular Biology of the Cell, 25(22):3461–3465, November 2014.

[10] Milestone 21 : Nature Milestones in Light Microscopy.

[11] Malte Renz. Fluorescence microscopyA historical and technical perspective. Cytometry Part A, 83(9):767–779, September 2013.

[12] Kurt Thorn. A quick guide to light microscopy in cell biology. Molecular Biology of the Cell, 27(2):219–222, January 2016.

[13] J. McIntosh and Thomas Hays. A Brief History of Research on Mitotic Mechanisms. Biology, 5(4):55, December 2016.

[14] Bruce Alberts, editor. Essential cell biology. Garland Science, New York, 3rd ed edition, 2009.

[15] Natalie J. Nannas and Andrew W. Murray. Tethering Sister Centromeres to Each Other Suggests the Spindle Checkpoint Detects Stretch within the Kinetochore. PLoS Genetics, 10(8):e1004492, August 2014.

[16] Robert Blackwell, Oliver Sweezy-Schindler, Christopher Edelmaier, Zachary R. Gergely, Patrick J. Flynn, Salvador Montes, Ammon Crapo, Alireza Doostan, J. Richard McIntosh, Matthew A. Glaser, and Meredith D. Betterton. Contributions of Microtubule Dynamic Instability and Rotational Diffusion to Kinetochore Capture. Biophysical Journal, September 2016.

[17] Adrianna S. Rodriguez, Alison N. Killilea, Joseph Batac, Jason Filopei, Dimitre Simeonov, Ida Lin, and Janet L. Paluh. Protein complexes at the microtubule organizing center regulate bipolar spindle assembly. Cell Cycle, 7(9):1246–1253, 2008.

[18] Yingchun Li and Eric C. Chang. Schizosaccharomyces pombe Ras1 effector, Scd1, interacts with Klp5 and Klp6 kinesins to mediate cytokinesis. Genetics, 165(2):477–488, 2003.

[19] Jason M. Sheltzer, Julie H. Ko, John M. Replogle, Nicole C. Habibe Burgos, Erica S. Chung, Colleen M. Meehl, Nicole M. Sayles, Verena Passerini, Zuzana Storchova, and Angelika Amon. Single-chromosome Gains Commonly Function as Tumor Suppressors. Cancer Cell, January 2017.

[20] Tamara Potapova and Gary Gorbsky. The Consequences of Chromosome Segregation Errors in Mitosis and Meiosis. Biology, 6(1):12, February 2017.

[21] Patrick G. Morris and Monica N. Fornier. Microtubule Active Agents: Beyond the Taxane Frontier. Clinical Cancer Research, 14(22):7167–7172, November 2008.

[22] Stephen J Haggarty, Thomas U Mayer, David T Miyamoto, Reza Fathi, Randall W King, Timothy J Mitchison, and Stuart L Schreiber. Dissecting cellular processes using small molecules: identification of colchicine-like, taxol-like and other small molecules that perturb mitosis. Chemistry & Biology, 7(4):275–286, April 2000.

[23] Corwin Hansch and Rajeshwar P. Verma. Understanding Tubulin/MicrotubuleTaxane Interactions: A Quantitative StructureActivity Relationship Study. Molecular Pharmaceutics, 5(1):151–161, February 2008.

[24] Barbara T. McGrogan, Breege Gilmartin, Desmond N. Carney, and Amanda McCann. Taxanes, microtubules and chemoresistant breast cancer. Biochimica et Biophysica Acta (BBA) - Reviews on Cancer, 1785(2):96–132, April 2008.

[25] Francesco Pampaloni, Gianluca Lattanzi, Alexandr Jon, Thomas Surrey, Erwin Frey, and Ernst-Ludwig Florin. Thermal fluctuations of grafted microtubules provide evidence of a length-dependent persistence length. Proceedings of the National Academy of Sciences, 103(27):10248–10253, July 2006.

[26] Flexural rigidity of microtubules and actin filaments measured from thermal fluctuations in shape. The Journal of Cell Biology, 120(4):923–934, February 1993.

[27] Clare M Waterman-Storer and ED Salmon. Positive feedback interactions between microtubule and actin dynamics during cell motility. Current Opinion in Cell Biology, 11(1):61–67, February 1999.

[28] Patricia T. Yam, Cyrus A. Wilson, Lin Ji, Benedict Hebert, Erin L. Barnhart, Natalie A. Dye, Paul W. Wiseman, Gaudenz Danuser, and Julie A. Theriot. Actinmyosin network reorganization breaks symmetry at the cell rear to spontaneously initiate polarized cell motility. J Cell Biol, 178(7):1207–1221, September 2007.

[29] Howard C. Berg and Robert A. Anderson. Bacteria Swim by Rotating their Flagellar Filaments. Nature, 245(5425):380–382, October 1973.

[30] Howard C. Berg. The Rotary Motor of Bacterial Flagella. Annual Review of Biochemistry, 72(1):19–54, 2003.

[31] Steven M. Block, Bruce J. Schnapp, and Lawrence S. B. Goldstein. Bead Movement by Single Kinesin Molecules Studied with Optical Tweezers. Nature; London, 348(6299):348–52, November 1990.

[32] Iain M. Cheeseman and Arshad Desai. Molecular architecture of the kinetochoremicrotubule interface. Nature Reviews Molecular Cell Biology, 9(1):33–46, January 2008.

[33] Xingkun Liu, Ian McLeod, Scott Anderson, John R. Yates, and Xiangwei He. Molecular analysis of kinetochore architecture in fission yeast. The EMBO Journal, 24(16):2919–2930, August 2005.

[34] Beth A. A. Weaver and Don W. Cleveland. Does aneuploidy cause cancer? Current Opinion in Cell Biology, 18(6):658–667, December 2006.

[35] Mo Yamada and Gohta Goshima. Mitotic Spindle Assembly in Land Plants: Molecules and Mechanisms. Biology, 6(1):6, January 2017.

[36] Tarun Kapoor. Metaphase Spindle Assembly. Biology, 6(1):8, February 2017.

[37] Akira Yamashita, Masamitsu Sato, Akiko Fujita, Masayuki Yamamoto, and Takashi Toda. The Roles of Fission Yeast Ase1 in Mitotic Cell Division, Meiotic Nuclear Oscillation, and Cytokinesis Checkpoint Signaling. Molecular Biology of the Cell, 16(3):1378–1395, March 2005.

[38] Ronald D. Vale, Thomas S. Reese, and Michael P. Sheetz. Identification of a novel force-generating protein, kinesin, involved in microtubule-based motility. Cell, 42(1):39–50, 1985.

[39] Clemens Valens. A really friendly guide to wavelets. ed. Clemens Valens, 1999.

[40] Anna Akhmanova and Michel O. Steinmetz. Tracking the ends: a dynamic protein network controls the fate of microtubule tips. Nature Reviews Molecular Cell Biology, 9(4):309–322, April 2008.

[41] Tim Mitchison and Marc Kirschner. Dynamic instability of microtubule growth. Nature, 312(5991):237–242, November 1984.

[42] Iana Kalinina, Amitabha Nandi, Petrina Delivani, Mariola R. Chacn, Anna H. Klemm, Damien Ramunno-Johnson, Alexander Krull, Benjamin Lindner, Nenad Pavin, and Iva M. Toli-Nrrelykke. Pivoting of microtubules around the spindle pole accelerates kinetochore capture. Nature Cell Biology, 15(1):82–87, January 2013.

[43] Marileen Dogterom and Stanislas Leibler. Physical aspects of the growth and regulation of microtubule structures. Physical review letters, 70(9):1347, 1993.

[44] Meredith Johnson Sagolla, Satoru Uzawa, and W. Zacheus Cande. Individual microtubule dynamics contribute to the function of mitotic and cytoplasmic arrays in fission yeast. Journal of Cell Science, 116(Pt 24):4891–4903, December 2003.

[45] Weng-Kian Tham, Hugo Ferretti, and Aephraim M. Steinberg. Beating Rayleigh's Curse by Imaging Using Phase Information. Physical Review Letters, 118(7):070801, February 2017.

[46] Jeff W. Lichtman and Jos-Angel Conchello. Fluorescence microscopy. Nature Methods, 2(12):910–919, December 2005.

[47] Peter J. Shaw and David J. Rawlins. The point-spread function of a confocal microscope: its measurement and use in deconvolution of 3-D data. Journal of Microscopy, 163(2):151–165, August 1991.

[48] Eva-Maria Mandelkow, Eckhard Mandelkow, and Ronald A. Milligan. Microtubule dynamics and microtubule caps: a time-resolved cryo-electron microscopy study. The Journal of cell biology, 114(5):977–991, 1991.

[49] Ronald E. Gordon. Electron microscopy: a brief history and review of current clinical application. Methods in Molecular Biology (Clifton, N.J.), 1180:119–135, 2014.

[50] Eric Betzig, George H. Patterson, Rachid Sougrat, O. Wolf Lindwasser, Scott Olenych, Juan S. Bonifacino, Michael W. Davidson, Jennifer Lippincott-Schwartz, and Harald F. Hess. Imaging Intracellular Fluorescent Proteins at Nanometer Resolution. Science, 313(5793):1642–1645, September 2006.

[51] Stefan W. Hell. Far-Field Optical Nanoscopy. Science, 316(5828):1153–1158, May 2007.

[52] Mary Osborn and Klaus Weber. Chapter 7 Immunofluorescence and Immunocytochemical Procedures with Affinity Purified Antibodies: Tubulin-Containing Structures. Methods in Cell Biology, 24:97–132, January 1982.

[53] Roger Y. Tsien. The green fluorescent protein. Annual review of biochemistry, 67(1):509–544, 1998.

[54] Douglas C. Prasher, Virginia K. Eckenrode, William W. Ward, Frank G. Prendergast, and Milton J. Cormier. Primary structure of the Aequorea victoria green-fluorescent protein. Gene, 111(2):229–233, February 1992.

[55] Lei S. Qi, Matthew H. Larson, Luke A. Gilbert, Jennifer A. Doudna, Jonathan S. Weissman, Adam P. Arkin, and Wendell A. Lim. Repurposing CRISPR as an RNA-Guided Platform for Sequence-Specific Control of Gene Expression. Cell, 152(5):1173–1183, February 2013.

[56] Nathan C Shaner, Paul A Steinbach, and Roger Y Tsien. A guide to choosing fluorescent proteins. Nature Methods, 2(12):905–909, December 2005.

[57] Paul S. Maddox, Kerry S. Bloom, and E. D. Salmon. The polarity and dynamics of microtubule assembly in the budding yeast Saccharomyces cerevisiae. Nature cell biology, 2(1):36–41, 2000.

[58] Kenneth E. Sawin and P. T. Tran. Cytoplasmic microtubule organization in fission yeast. Yeast, 23(13):1001–1014, October 2006.

[59] D. Axelrod, D. E. Koppel, J. Schlessinger, E. Elson, and W. W. Webb. Mobility measurement by analysis of fluorescence photobleaching recovery kinetics. Biophysical Journal, 16(9):1055–1069, September 1976.

[60] Daniel Wstner, Lukasz M. Solanko, Frederik W. Lund, Daniel Sage, Hans J. Schroll, and Michael A. Lomholt. Quantitative fluorescence loss in photobleaching for analysis of protein transport and aggregation. BMC bioinformatics, 13(1):296, 2012.

[61] D. L. Andrews. A unified theory of radiative and radiationless molecular energy transfer. Chemical Physics, 135(2):195–201, August 1989.

[62] Ammasi Periasamy. Fluorescence resonance energy transfer microscopy: a mini review. Journal of Biomedical Optics, 6(3):287–291, 2001.

[63] Elizabeth A. Jares-Erijman and Thomas M. Jovin. FRET imaging. Nature Biotechnology, 21(11):1387–1395, November 2003.

[64] J. M. Mitchison and P. Nurse. Growth in cell length in the fission yeast Schizosaccharomyces pombe. Journal of Cell Science, 75(1):357–376, April 1985.

[65] J. M. Mitchison and K. M. Wilbur. The incorporation of protein and carbohydrate precursors during the cell cycle of a fission yeast. Experimental Cell Research, 26(1):144–157, February 1962.

[66] Peter A. Fantes and Charles S. Hoffman. A Brief History of Schizosaccharomyces pombe Research: A Perspective Over the Past 70 Years. Genetics, 203(2):621–629, June 2016.

[67] Paul Nurse and Yvonne Bissett. Gene required in G1 for commitment to cell cycle and in G2 for control of mitosis in fission yeast. Nature, 292(5823):558–560, August 1981.

[68] Paul Russell and Paul Nurse. cdc25+ functions as an inducer in the mitotic control of fission yeast. Cell, 45(1):145–153, April 1986.

[69] Kathleen L. Gould and Paul Nurse. Tyrosine phosphorylation of the fission yeast cdc2+ protein kinase regulates entry into mitosis. Nature, 342(6245):39–45, November 1989.

[70] Iain Hagan and Mitsuhiro Yanagida. Kinesin-related cut 7 protein associates with mitotic and meiotic spindles in fission yeast. Nature, 356(6364):74–76, March 1992.

[71] Takeo Tanaami, Shinya Otsuki, Nobuhiro Tomosada, Yasuhito Kosugi, Mizuho Shimizu, and Hideyuki Ishida. High-speed 1-frame/ms scanning confocal microscope with a microlens and Nipkow disks. Applied Optics, 41(22):4704–4708, August 2002.

[72] Nicolas Chenouard, Ihor Smal, Fabrice de Chaumont, Martin Maka, Ivo F. Sbalzarini, Yuanhao Gong, Janick Cardinale, Craig Carthel, Stefano Coraluppi, Mark Winter, Andrew R. Cohen, William J. Godinez, Karl Rohr, Yannis Kalaidzidis, Liang Liang, James Duncan, Hongying Shen, Yingke Xu, Klas E. G. Magnusson, Joakim Jaldn, Helen M. Blau, Perrine Paul-Gilloteaux, Philippe Roudot, Charles Kervrann, Franois Waharte, Jean-Yves Tinevez, Spencer L. Shorte, Joost Willemse, Katherine Celler, Gilles P. van Wezel, Han-Wei Dan, Yuh-Show Tsai, Carlos Ortiz de Solrzano, Jean-Christophe Olivo-Marin, and Erik Meijering. Objective comparison of particle tracking methods. Nature Methods, 11(3):281–289, March 2014.

[73] John C. Russ. The image processing handbook. CRC press, 2016.

[74] Christopher M. Bishop. Pattern recognition and machine learning. Information science and statistics. Springer, New York, 2006.

[75] Alexei O. Demchouk, Melissa K. Gardner, and David J. Odde. Microtubule Tip Tracking and Tip Structures at the Nanometer Scale Using Digital Fluorescence Microscopy. Cellular and Molecular Bioengineering, 4(2):192–204, June 2011.

[76] Louis S. Prahl, Brian T. Castle, Melissa K. Gardner, and David J. Odde. Quantitative Analysis of Microtubule Self-assembly Kinetics and Tip Structure. In Methods in Enzymology, volume 540, pages 35–52. Elsevier, 2014.

[77] K. Jaqaman, J. F. Dorn, E. Marco, P. K. Sorger, and G. Danuser. Phenotypic clustering of yeast mutants based on kinetochore microtubule dynamics. Bioinformatics, 23(13):1666–1673, July 2007.

[78] Khuloud Jaqaman, Dinah Loerke, Marcel Mettlen, Hirotaka Kuwata, Sergio Grinstein, Sandra L Schmid, and Gaudenz Danuser. Robust single-particle tracking in live-cell time-lapse sequences. Nature Methods, 5(8):695–702, August 2008.

[79] Roy Jonker and Anton Volgenant. A shortest augmenting path algorithm for dense and sparse linear assignment problems. Computing, 38(4):325–340, 1987.

[80] W. M. Young and E. W. Elcock. Monte Carlo studies of vacancy migration in binary ordered alloys: I. Proceedings of the Physical Society, 89:735–746, November 1966.

[81] L.E. Hough, Anne Schwabe, Matthew A. Glaser, J. Richard McIntosh, and M.D. Betterton. Microtubule Depolymerization by the Kinesin-8 Motor Kip3p: A Mathematical Model. Biophysical Journal, 96(8):3050–3064, April 2009.

[82] C. S. Hoffman, V. Wood, and P. A. Fantes. An Ancient Yeast for Young Geneticists: A Primer on the Schizosaccharomyces pombe Model System. Genetics, 201(2):403–423, October 2015.

[83] A. Unsworth, H. Masuda, S. Dhut, and T. Toda. Fission Yeast Kinesin-8 Klp5 and Klp6 Are Interdependent for Mitotic Nuclear Retention and Required for Proper Microtubule Dynamics. Molecular Biology of the Cell, 19(12):5104–5115, December 2008.

[84] Masashi Yukawa, Chiho Ikebe, and Takashi Toda. The Msd1Wdr8Pkl1 complex anchors microtubule minus ends to fission yeast spindle pole bodies. The Journal of Cell Biology, 209(4):549–562, May 2015.

[85] Susan M. Baker, Robert W. Buckheit, and Matthias M. Falk. Green-to-red photoconvertible fluorescent proteins: tracking cell and protein dynamics on standard wide-field mercury arc-based microscopes. BMC cell biology, 11(1):15, 2010.

[86] Eugene V. Koonin. A conserved ancient domain joins the growing superfamily of 35 exonucleases. Current Biology, 7(10):R604–R606, 1997.

[87] Michael B. Elowitz, Michael G. Surette, Pierre-Etienne Wolf, Jeff Stock, and Stanislas Leibler. Photoactivation turns green fluorescent protein red. Current Biology, 7(10):809–812, 1997.

[88] Jeffrey N. Molk, Scott C. Schuyler, Jenny Y. Liu, James G. Evans, Edward D. Salmon, David Pellman, and Kerry Bloom. The differential roles of budding yeast Tem1p, Cdc15p, and Bub2p protein dynamics in mitotic exit. Molecular biology of the cell, 15(4):1519–1532, 2004.

[89] A. Carpy, K. Krug, S. Graf, A. Koch, S. Popic, S. Hauf, and B. Macek. Absolute Proteome and Phosphoproteome Dynamics during the Cell Cycle of Schizosaccharomyces pombe (Fission Yeast). Molecular & Cellular Proteomics, 13(8):1925–1936, August 2014.

[90] Edward H. Adelson. William T. Freeman Edward H. Adelson y. 1991.

[91] P. R. Christensen. Morphology and Composition of the Surface of Mars: Mars Odyssey THEMIS Results. Science, 300(5628):2056–2061, June 2003.

[92] J.-Q. Wu. Counting Cytokinesis Proteins Globally and Locally in Fission Yeast. Science, 310(5746):310–314, October 2005.

[93] Adi L. Tarca, Vincent J. Carey, Xue-wen Chen, Roberto Romero, and Sorin Drghici. Machine learning and its applications to biology. PLoS Comput Biol, 3(6):e116, 2007.

[94] Richard Durbin, editor. Biological sequence analysis: probabalistic models of proteins and nucleic acids. Cambridge University Press, Cambridge, UK : New York, 1998.

[95] Ramon van Handel. Hidden markov models. Unpublished notes, 2008.

[96] BEN NORDSTROM. FINITE MARKOV CHAINS. 2008.

[97] Nikolay Perunov, Robert A. Marsland, and Jeremy L. England. Statistical Physics of Adaptation. Physical Review X, 6(2), June 2016.

[98] William Edwards Deming and S. L. Morgan. Preface to the second edition. Elsevier, 1993.

[99] Alphan Altinok, Motaz El-Saban, Austin J. Peck, Leslie Wilson, Stuart C. Feinstein, B. S. Manjunath, and Kenneth Rose. Activity analysis in microtubule videos by mixture of hidden Markov models. In Computer Vision and Pattern Recognition, 2006 IEEE Computer Society Conference on, volume 2, pages 1662–1669. IEEE, 2006.

[100] Carl Burch. A survey of machine learning. Tech. report, Pennsylvania Governor's School for the Sciences, 2001.

[101] Natalie J. Nannas, Eileen T. OToole, Mark Winey, and Andrew W. Murray. Chromosomal attachments set length and microtubule number in the Saccharomyces cerevisiae mitotic spindle. Molecular biology of the cell, 25(25):4034–4048, 2014.

[102] Aaron Novick and Milton Weiner. Enzyme induction as an all-or-none phenomenon. Proceedings of the National Academy of Sciences, 43(7):553–566, 1957.

[103] Aaron M. Streets, Ang Li, Tao Chen, and Yanyi Huang. Imaging without Fluorescence: Nonlinear Optical Microscopy for Quantitative Cellular Imaging. Analytical Chemistry, 86(17):8506–8513, September 2014.

[104] Carsten Grashoff, Brenton D. Hoffman, Michael D. Brenner, Ruobo Zhou, Maddy Parsons, Michael T. Yang, Mark A. McLean, Stephen G. Sligar, Christopher S. Chen, Taekjip Ha, and Martin A. Schwartz. Measuring mechanical tension across vinculin reveals regulation of focal adhesion dynamics. Nature, 466(7303):263–266, July 2010.

[105] T. F. Cootes, G. J. Edwards, and C. J. Taylor. Active appearance models. IEEE Transactions on Pattern Analysis and Machine Intelligence, 23(6):681–685, June 2001.

[106] Michelle L. James and Sanjiv S. Gambhir. A Molecular Imaging Primer: Modalities, Imaging Agents, and Applications. Physiological Reviews, 92(2):897–965, April 2012.

[107] Minghua Xu and Lihong V. Wang. Photoacoustic imaging in biomedicine. Review of Scientific Instruments, 77(4):041101, April 2006.

[108] Takashi Akera, Yuhei Goto, Masamitsu Sato, Masayuki Yamamoto, and Yoshinori Watanabe. Mad1 promotes chromosome congression by anchoring a kinesin motor to the kinetochore. Nature Cell Biology, 17(9):1124–1133, September 2015.

[109] Simon Gordonov, Mun Kyung Hwang, Alan Wells, Frank B. Gertler, Douglas A. Lauffenburger, and Mark Bathe. Time Series Modeling of Live-Cell Shape Dynamics for Image-based Phenotypic Profiling. Integrative biology : quantitative biosciences from nano to macro, 8(1):73–90, January 2016.

[110] E. Meijering, I. Smal, and G. Danuser. Tracking in molecular bioimaging. IEEE Signal Processing Magazine, 23(3):46–53, May 2006.

[111] Bungo Akiyoshi, Krishna K. Sarangapani, Andrew F. Powers, Christian R. Nelson, Steve L. Reichow, Hugo Arellano-Santoyo, Tamir Gonen, Jeffrey A. Ranish, Charles L. Asbury, and Sue Biggins. Tension directly stabilizes reconstituted kinetochore-microtubule attachments. Nature, 468(7323):576–579, November 2010.

[112] Charles Asbury. Anaphase A: Disassembling Microtubules Move Chromosomes toward Spindle Poles. Biology, 6(1):15, February 2017.

[113] Ajit Joglekar. A Cell Biological Perspective on Past, Present and Future Investigations of the Spindle Assembly Checkpoint. Biology, 5(4):44, November 2016.

[114] Michael Lampson and Ekaterina Grishchuk. Mechanisms to Avoid and Correct Erroneous Kinetochore-Microtubule Attachments. Biology, 6(1):1, January 2017.

[115] Helder Maiato, Ana Gomes, Filipe Sousa, and Marin Barisic. Mechanisms of Chromosome Congression during Mitosis. Biology, 6(1):13, February 2017.

[116] Thomas J. Maresca and E. D. Salmon. Welcome to a new kind of tension: translating kinetochore mechanics into a wait-anaphase signal. Journal of Cell Science, 123(Pt 6):825–835, March 2010.

[117] Ronald D. Vale and Ronald A. Milligan. The Way Things Move: Looking Under the Hood of Molecular Motor Proteins. Science, 288(5463):88–95, April 2000.

[118] Kendra S. Burbank and Timothy J. Mitchison. Microtubule dynamic instability. Current Biology, 16(14):R516–R517, July 2006.

[119] RonaldE. Gordon. Electron Microscopy: A Brief History and Review of Current Clinical Application. In Christina E. Day, editor, Histopathology, number 1180 in Methods in Molecular Biology, pages 119–135. Springer New York, January 2014. DOI: 10.1007/978-1-4939-1050-2_7.